Discrete Green's functions for unbounded domains using finite element method

B. Boroomand
F. Mossaiby

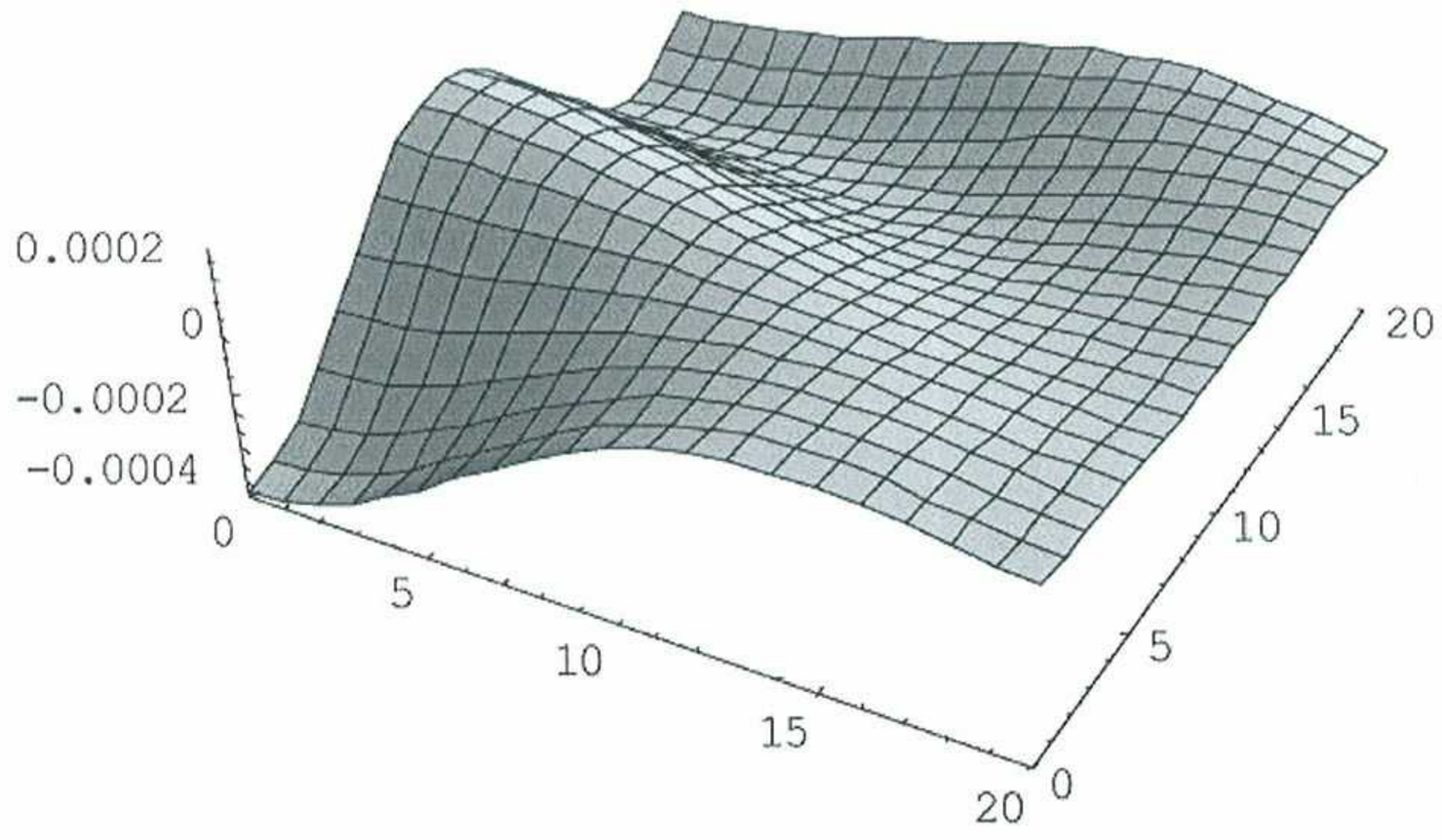

Publication CIMNE Nº-267, May 2005

Discrete Green's functions for unbounded domains using finite element method

B. Boroomand
F. Mossaiby

Publication CIMNE Nº-267, May 2005

International Center for Numerical Methods in Engineering
Gran Capitán s/n, 08034 Barcelona, Spain

Discrete Green's functions for unbounded domains using finite element method

B. Boroomand[1] and F. Mossaiby[2]

Civil Engineering Department, Isfahan University of Technology, Isfahan 84156-83111, Iran
Email: boromand@cc.iut.ac.ir

Abstract

In this report dynamic solution of unbounded domains using pure finite element method is presented. The problems of concern are those with governing differential equations of constant coefficient. When the grid is of repeatable pattern the solution of an unbounded domain is reducible to a solution over a smaller domain with a grid consisting of few numbers of repeatable patterns. It is shown that by use of the proportionality property, having roots in governing equations, both conditions required for a unique solution, i.e. the decay and radiation of energy, are met through a spectral formulation. As a key point, a consistent transformation approach is proposed in order to employ such a spectral formulation for the solution. The transformation technique is analogous to those conventionally used for solution of partial differential equations but of course in a matrix form. To demonstrate the applicability of the method, Green's functions for two dimensional scalar and elastic wave equations are obtained numerically in frequency domain. The method is also capable of giving Green's functions for dynamic solution of domains with repeatable material properties. Comprehensive discussions are given for accuracy and convergence of the solution.

Keywords: *Unbounded domains, Discrete Green's functions, Discrete Wave Problems, Periodic Mesh Pattern*

---

[1] Associate Professor
[2] Graduate student

Contents

1. INTRODUCTION

The need for solution of mathematical models of unbounded domains arises in many engineering applications. Wave propagation in acoustic or magnetic fields and elastic waves in geophysics are the notable examples. There are several approaches for dynamic solution of unbounded domains. Boundary element/integral method is the most common method for such solutions when Green's functions are available. The Green's functions are usually found through direct solution of the governing differential equations using transformation techniques. Nevertheless, working with such functions, if exist, is not easy task because of inherent singularities.

In the context of finite element method, however, solution of unbounded domain may be performed by introducing infinite elements or artificial boundary conditions for a bounded region. A survey in the literature shows that both approaches are growing fast, though each has some advantages against the other.

In the category of using infinite elements the work by Bettess and Zienkiewicz [1,2] appears to be the pioneering one. In this approach the unbounded domain is replaced with a bounded one and elements with infinite length are constructed with use of some shape functions representing decay condition. The elements are sometimes called unconjugated infinite element in order to be distinguishable from their counterparts, known as conjugated infinite elements, in which some complex conjugates shape functions are used in the weighted residual method. The representative of the latter approach is the work due to Astley [3]. A good literature of the methods can be found in review papers [4, 5] and also reference [6].
In the category of using artificial boundary conditions the work due to Engquist and Majda in the late 1970s is recognized as a pioneering one [7]. In this form of approach the unbounded domain is again replaced with a bounded one but the effects of the remaining parts are taken into account through a series of energy absorbent boundary conditions. The concept has further been extended by others and thus the so called Dirichlet-to-Neumann mapping technique [8, 9] and Perfectly Matched Layer approaches [10, 11] were developed. A comparison between the performances of some classes of the infinite elements and artificial boundary conditions has been given in [12]. A good survey to the date of the methods may be found in reference [13].

The above mentioned methods are in fact solution treatments for using different element/boundary components at the bounded part of the domain. For behavior prediction of pure finite element models, i.e. models using finite element covering the entire unbounded domain, few studies can be traced in the literature. An early work on the subject is due to Thatcher in which the behavior of an infinite number of elements has been predicted in a systematic manner for a Laplace's equation [14]. A somewhat similar approach has been employed by Dasgupta [15], called cloning, and later by Wolf and Song [16], called multi-cell cloning, for dynamic solution of problems encountering in geophysics. These methods employ similarity effects in the geometry of the meshes. In the same line, Wolf and Song introduced another method, called "scaled boundary finite elements" [17]. The history of the method may be found in [18]. This latter approach employs finite element and boundary integral methods in circumferential and radial directions, respectively. The method may be considered in the category of infinite element approaches, nevertheless the main difference lies in the use of the exact solution along redial direction for the differential equations resulted from the geometrical similarity effect.

In this report we shall model the behavior of an infinite number of elements, supposing that the whole domain has been discretized into similar elements, on an area with finite number of the same elements. As a representative of such solutions we shall present the Green's functions in finite element sense. The numerically-evaluated Green's functions can readily be used in construction of absorbing energy

boundaries without much effort. This will also help to avoid the difficulties arising in integration of singular functions. It should be noted that the approach given in this report does not limit to solution with finite element method and any other numerical method can be employed in an analogous manner.

The layout of the report is as follows. In the next section the model problem and assumptions used are presented. Requirements for decay and radiation conditions are also discussed in the same section. In Section 3 we specify the wave problems which are considered in this report along with the finite element approach employed. The solution method suitable for unbounded domains via FEM is described in the same section. The new features including the spectral form of solution, the transformations used, treatment of the boundary conditions and application of the decay and radiation conditions in finite element sense are explained together with the solution method. In Section 4 some numerical results are given. In this latter section we present numerical presentation of Green's functions for unbounded scalar and elasticity problems where we discuss about the accuracy and convergence of the solutions. Overall conclusions from the application of the proposed method are given in Section 5.

2. MODEL PROBLEM

In this section we shall give some preliminary assumptions used for the governing equations and the unbounded domain.

Assumption I. We assume that the system of governing differential equation/equations is of constant coefficient.

As we describe later this assumption plays a key role in our solution technique and constitutes simplest form of repeatability in the numerical procedure. However, such a repeatability effect may be resulted from a system of equations with periodic variation of coefficients treating of which is beyond the scopes of this report and will be addressed in future works.

Numerous wave problems arising in physics or many problems in theory of diffusion fall within the category of problems with above assumption especially when the governing equations are written in Cartesian coordinates.

Assumption II. A Cartesian coordinate is used to define the mathematical model.

Most of wave equations in physics may be written as the following equation

$$\mathscr{L}\mathbf{U} - \rho\ddot{\mathbf{U}} = \mathbf{F}(x, y, t) \qquad (x, y) \in \mathbb{R}\times\mathbb{R} \tag{1}$$

where $\mathbf{U}$ and $\ddot{\mathbf{U}}$ are, respectively, vector of the main unknown functions and its second derivatives in time, $\mathscr{L}$ is an appropriate differential operator, which is elliptic in spatial coordinates and, in our case, is linear with constant coefficient, ρ is a material constant (e.g. density) and $\mathbf{F}(x, y, t)$ is the source term expressed as a function of spatial coordinates and time t. We note that the whole equation is of hyperbolic type in time domain. As is seen in this report we focus on two dimensional wave problems. The reader may also note that we have used notations with vector unknowns which are reducible to scalar problems as special cases.

When the solution of (1) is sought in time domain, usually the fundamental solution (Green's function) is first obtained through solution of the unbounded domain with unit impulse load defined at origin. In

that case the source term takes the form of Dirac Delta function in spatial coordinates as well as the time. The complete solutions for general source terms are then found through suitable integration of such fundamental solution in both spatial coordinates and time.

The solution of (1) may also be performed using Fourier transformation of the source term in time domain. In that case the fundamental solution is obtained in frequency domain with the aid of a source term as a Dirac Delta function just in spatial coordinates. The complete solution is then found through inverse Fourier transformation and suitable integration in spatial coordinates. In this report we shall give solutions to differential equations in frequency domain. Thus one may use

$$\mathbf{U} = \mathbf{u}e^{i\omega t} \tag{2}$$

while letting $\mathbf{u}$ be a vector of complex function. In Equation (2) ω is the frequency value and $i = \sqrt{-1}$. Substitution of (2) in (1) results in the following elliptic differential equation

$$\mathscr{L}\mathbf{u} + \rho\omega^2\mathbf{u} = \mathbf{f} \tag{3}$$

In which $\mathbf{f}$ is Fourier transformation of $\mathbf{F}$. If $\mathbf{u}$ is to be fundamental solution in frequency domain, the source term takes the form of

$$\mathbf{f} = \delta(x)\delta(y) \tag{4}$$

Where δ is Dirac Delta function. This means that we are dealing with following problem

$$\begin{cases} \mathscr{L}\mathbf{u} + \rho\omega^2\mathbf{u} = \mathbf{0} & x \neq 0 \quad y \neq 0 \\ \mathscr{L}\mathbf{u} + \rho\omega^2\mathbf{u} \neq \mathbf{0} & x = 0 \quad y = 0 \end{cases} \tag{5}$$

Usually, a quarter of the domain can be solved when appropriate boundary conditions are considered.

Assumption III. The unbounded domain is defined over a part of space with $x \geq 0$ and $y \geq 0$ for two dimensional problems (and $z \geq 0$ for three dimensional ones).

The third assumption helps to use just one of the cases in (5) and treat the effects of the source term as a point boundary condition. Therefore the problem is reduced to

$$\mathscr{L}\mathbf{u} + \rho\omega^2\mathbf{u} = \mathbf{0} \qquad (x, y) \in [0, \infty) \times [0, \infty) \tag{6}$$

with some additional conditions either on $\mathbf{u}$ or on the gradients of it at $x = 0$ and $y = 0$.

It can be seen that the main problem to be solved is a system of homogenous differential equations with specified boundary conditions. In the next sub-section we describe the proportionality property existing in constant coefficient differential equations.

2.1 The proportionality effect

In this section we describe an interesting property that exists in any system of differential equation with constant coefficients. From differential calculus we remember that the general form of solution for system of equation like (6) may be written as

$$\mathbf{u}(x,y)=\mathbf{A}e^{\alpha x+\beta y} \tag{7}$$

With $\mathbf{A}$, α and β being a vector of constants and two unspecified scalars, respectively. It may be seen that the following relations exist

$$\mathbf{u}(x+L_x,y)=\mathbf{A}e^{\alpha(x+L_x)+\beta y}=\mathbf{A}e^{(\alpha x+\beta y)+\alpha L_x}=\mathbf{A}e^{(\alpha x+\beta y)}e^{\alpha L_x}=\mu_{01}\mathbf{u}(x,y)$$

and

$$\mathbf{u}(x+nL_x,y)=\mathbf{A}e^{\alpha(x+nL_x)+\beta y}=\mathbf{A}e^{(\alpha x+\beta y)+n\alpha L_x}=\mathbf{A}e^{(\alpha x+\beta y)}e^{n\alpha L_x}=(\mu_{01})^n\mathbf{u}(x,y)$$

for x direction and similarly

$$\mathbf{u}(x,y+L_y)=\mathbf{A}e^{\alpha x+\beta(y+L_y)}=\mu_{02}\mathbf{u}(x,y)$$

and

$$\mathbf{u}(x,y+mL_y)=\mathbf{A}e^{\alpha x+\beta(y+mL_y)}=(\mu_{02})^m\mathbf{u}(x,y)$$

or more generally

$$\mathbf{u}(x+nL_x,y+mL_y)=\mathbf{A}e^{\alpha(x+nL_x)+\beta(y+mL_y)}=(\mu_{01})^n(\mu_{02})^m\mathbf{u}(x,y) \tag{8}$$

In above L_x and L_y are arbitrary lengths along x and y direction. Relation (8) states that for each spectral solution as (7) the values of components of vector $\mathbf{u}$ is proportional to the values of the vector at multiple length scale farther and the proportionality value varies exponentially with the order of the multiply number. This appealing effect is also seen even when the differential equations are written as the equivalent integral equations. In the forthcoming sections we shall refer to this effect when a weighted residual method is applied for numerical solution.

We further note that substitution of (7) in (6) leads to a system of equations like

$$\mathbf{L}\mathbf{A}e^{\alpha x+\beta y}=\mathbf{0} \quad \text{or} \quad \mathbf{L}\mathbf{A}=\mathbf{0} \tag{9}$$

In which $\mathbf{L}$ is a matrix containing functions of coefficients α and β. A non-trivial solution for such a system of equation is found as null space of $\mathbf{L}$ by letting its determinant be zero, i.e.

$$|\mathbf{L}|=0. \tag{10}$$

This results in a characteristic equation with α and β as the main variables. Now one variable can be found in terms of the other as $\beta=f(\alpha)$ or $\alpha=g(\beta)$. We note that depending on the order of the characteristic equation, there may be more than one relation in each case.

The general solution of the problem may be written as the superposition of spectral solutions, for instance when β is found in terms of α, as

$$\mathbf{u} = \int_{\alpha} \sum_{i} \mathbf{A}_i e^{\alpha x + \beta_i y} d\alpha = \int_{\alpha} \sum_{i} \mathbf{A}_i e^{\alpha x + f_i(\alpha) y} d\alpha \qquad (11)$$

Where inner summation is taken over null space bases of $\mathbf{L}$ and the outer integration is performed over all feasible values of α .

2.2 The decay and radiation conditions

Before explaining the numerical solution technique it is worthwhile to address the decay and radiation condition for wave propagation problems.

Decay condition: Noting that the domain is defined as $x \geq 0$ and $y \geq 0$, and provided that the exponents n and m in relation (8) are nonnegative integers then the decay condition is expressed as

$$|\mu_{01}| < 1 \quad \text{and} \quad |\mu_{02}| < 1 \qquad (12)$$

Conditions (12) ensure that $\mathbf{u} \to \mathbf{0}$ as $n \to \infty$ or $m \to \infty$. It should be noted that $\mathbf{u}$ is the amplitude of $\mathbf{U}$ as stated in (2) and clearly $\mathbf{U} \to 0$ as $n, m \to \infty$ since $e^{i\omega t}$ is a bounded periodic function.

We also note that μ_{01} and μ_{02} can generally be complex values and thus each condition of (12) defines a circle in Gaussian plane.

Radiation condition: Apart from the decay condition, in wave propagation problem the radiation condition must be met. Physical interpretation of the phenomenon is that the energy going towards infinity never comes back or be reflected. Representative of the traveling energy is in fact the wave or the traveling deformation. Therefore it is necessary to ensure that the function representing the deformation in time show such out going movements of energy.

Substitution of (7) in (2) leads to

$$\mathbf{U} = \mathbf{A} e^{\alpha x + \beta y + i\omega t} \qquad (13)$$

Now supposing that α and β generally take the form of

$$\alpha = a + ib \quad \text{and} \quad \beta = c + id \qquad (14)$$

Then

$$\mathbf{U} = \mathbf{A} e^{(a+ib)x + (c+id)y + i\omega t} = \mathbf{A} e^{ax+cy} e^{i(bx+dy+\omega t)} \qquad (15)$$

It can be seen that for outgoing waves following conditions must be met

$$a < 0 \,,\; c < 0 \,,\; b < 0 \;\text{ and }\; d < 0 \qquad (16)$$

The first two conditions are in fact reflecting the decay condition as the first two terms in the last expression in (15) play the role of amplitude at point (x, y). However, the third term in the right hand side of (15) defines the direction of the movement. From above discussion it is concluded that the proportionality values in x and y direction take the forms of

$$\mu_{01} = e^{-|a|L_x} e^{-i|b|L_x} \qquad \text{and} \qquad \mu_{02} = e^{-|c|L_y} e^{-i|d|L_y} \tag{17}$$

Since L_x and L_y are arbitrary lengths we may take $L_x \,|\, b \,| \leq \frac{\pi}{2}$ and $L_y \,|\, b \,| \leq \frac{\pi}{2}$. This leads to

$$\Re(\mu_{01}).\Im(\mu_{01}) < 0 \quad , \quad \Re(\mu_{02}).\Im(\mu_{02}) < 0 \tag{18}$$

where $\Re(.)$ and $\Im(.)$ refer to the real and imaginary parts of the quantity. These two conditions ensure the radiation condition in the directions of the main axes. This means that feasible domains are the second and forth quadrants of the unit-radius circle over the Gaussian plane.

REMARK 1. In wave problems quantities $|b|$ and $|d|$ represent the values of $\frac{2\pi}{\lambda_x}$ and $\frac{2\pi}{\lambda_y}$ with λ_x and λ_y being the associated wave lengths along x and y. From relation $L_x \,|\, b \,| \leq \frac{\pi}{2}$ and $L_y \,|\, b \,| \leq \frac{\pi}{2}$ one can conclude that

$$L_x < \frac{\lambda_x}{4} \quad \text{and} \quad L_y < \frac{\lambda_y}{4}$$

It can be concluded that the best presentation of radiation condition can be seen when the periodic lengths are considered less than a quarter of the associated wave lengths.

□

In forthcoming sections we shall frequently refer to inequalities of (18) as the radiation condition for the solution technique.

3. THE WAVE PROBLEMS AND THE SOLUTION TECHNIQUE

Before explaining the formulation of the numerical solution, we prefer to choose particular form of widely used differential operator as

$$\mathscr{L} \equiv \mathbf{S}^T \mathbf{D} \mathbf{S} \tag{19}$$

In which $\mathbf{S}$ is a differential operator and $\mathbf{D}$ is material modulus matrix. Then the differential equation (6) takes the form of

$$\mathbf{S}^T \mathbf{D} \mathbf{S} \mathbf{u} + \rho\omega^2 \mathbf{u} = \mathbf{0} \tag{20}$$

For elastic or scalar wave two dimensional problems operator $\mathbf{S}$ and matrix $\mathbf{D}$ are defined as

For elastic wave problems (plane strain)

$$\mathbf{S}=\begin{bmatrix}\dfrac{\partial}{\partial x} & 0\\ 0 & \dfrac{\partial}{\partial y}\\ \dfrac{\partial}{\partial y} & \dfrac{\partial}{\partial x}\end{bmatrix} \qquad \mathbf{D}=\frac{(1-\nu)E}{(1+\nu)(1-2\nu)}\begin{bmatrix}1 & \dfrac{\nu}{1-\nu} & 0\\ \dfrac{\nu}{1-\nu} & 1 & 0\\ 0 & 0 & \dfrac{1-2\nu}{2(1-\nu)}\end{bmatrix} \tag{21}$$

For scalar wave problems

$$\mathbf{S}=\begin{bmatrix}\dfrac{\partial}{\partial x}\\ \dfrac{\partial}{\partial y}\end{bmatrix} \qquad \mathbf{D}=\begin{bmatrix}k_x & 0\\ 0 & k_y\end{bmatrix} \tag{22}$$

With E and ν being elastic modulus and Poisson's ratio for elastic material and k_x and k_y conductivity coefficient along x and y, respectively.

It is noteworthy that orthotropic material may also be used by replacing the $\mathbf{D}$ matrix and, as long as the system of differential equations remains linear with constant coefficients, this does not affect the methodology explained later.

As mentioned in the introduction, in this report we shall employ the finite element method for numerical solution. It should be emphasized again that the approach given in this report does not limit to finite element method. In the next subsection we shall give the finite element formulation of the problem.

3.1 Finite element analysis

The finite element solution of (20) starts with discretization of the domain and approximation of $\mathbf{u}$ as

$$\mathbf{u}\approx\mathbf{u}_h=\mathbf{N}\bar{\mathbf{u}} \tag{23}$$

where $\bar{\mathbf{u}}$ are nodal values of the approximate function and $\mathbf{N}$ is an appropriate set of shape functions. Application of Galerkin form of weighted residual method leads to

$$\int_\Omega \mathbf{N}^T\left\{\mathbf{S}^T\mathbf{D}\mathbf{S}\left(\mathbf{N}\bar{\mathbf{u}}\right)+\rho\omega^2\mathbf{N}\bar{\mathbf{u}}\right\}d\Omega=\mathbf{0} \tag{24}$$

Although we can continue with above strong formulation, in standard finite element it is usually preferred to employ weak form of (24) in order to take advantage of shape functions with C^0 continuity. Thus the first integration in (24) is taken by part and the equation is rearranged as following well known formulation

$$-\left(\int_{\Omega}(\mathbf{SN})^T\mathbf{D}(\mathbf{SN})d\Omega\right)\bar{\mathbf{u}}+\rho\omega^2\left(\int_{\Omega}\mathbf{N}^T\mathbf{N}d\Omega\right)\bar{\mathbf{u}}+\int_{\Gamma_\sigma}\mathbf{N}^T(\tilde{\mathbf{n}}\mathbf{DSN}\bar{\mathbf{u}})d\Gamma=\mathbf{0} \tag{25-a}$$

or

$$\left(\int_{\Omega}\mathbf{B}^T\mathbf{DB}d\Omega\right)\bar{\mathbf{u}}-\rho\omega^2\left(\int_{\Omega}\mathbf{N}^T\mathbf{N}d\Omega\right)\bar{\mathbf{u}}-\int_{\Gamma_\sigma}\mathbf{N}^T(\tilde{\mathbf{n}}\mathbf{DB}\bar{\mathbf{u}})d\Gamma=\mathbf{0} \tag{25-b}$$

in which $\mathbf{B}=\mathbf{SN}$ and $\tilde{\mathbf{n}}$ is a matrix containing components of unit normal to the boundary arranged in an appropriate form for scalar and elastic wave problems. In relations (25) Γ_σ denotes the boundaries with Neumann conditions and the last integration in (25) plays the role of external forces since the tractions of approximate solution are considered to be equal to those of exact gradient field

$$\tilde{\mathbf{n}}\mathbf{DB}\bar{\mathbf{u}}=\mathbf{t} \quad \text{on} \quad \Gamma_\sigma \tag{26}$$

where $\mathbf{t}$ is the vector of exact tractions. For the model problems in this report Neumann boundaries Γ_σ, if exist, are considered at $x=0$ and/or $y=0$. Essential boundary conditions with prescribed values for $\mathbf{u}$ as $\mathbf{u}|_{\Gamma_u}=\mathbf{u}_B$ are also considered at $x=0$ and/or $y=0$, if exist. Using conventional notation

$$\mathbf{K}=\int_{\Omega}\mathbf{B}^T\mathbf{DB}d\Omega \;, \quad \mathbf{M}=\rho\int_{\Omega}\mathbf{N}^T\mathbf{N}d\Omega \quad \text{and} \quad \mathbf{f}_t=\int_{\Gamma_\sigma}\mathbf{N}^T\mathbf{t}d\Gamma \tag{27}$$

then equation (25-b) becomes

$$\left(\mathbf{K}-\omega^2\mathbf{M}\right)\bar{\mathbf{u}}=\mathbf{f}_t \tag{28-a}$$

or

$$\mathbf{K}_d\bar{\mathbf{u}}=\mathbf{f}_t \;, \quad \mathbf{K}_d=\mathbf{K}-\omega^2\mathbf{M} \tag{28-b}$$

Equation (28-b) is in fact representing the dynamic equilibrium equation of the system in finite element sense. The system of equation consists of infinite number of degrees of freedoms and the solution must be found with boundary conditions specified at $x=0$ and $y=0$, and also the decay and radiation conditions as $x, y \to \infty$.

The solution of (28-b) is generally impossible unless some additional assumptions are made for reduction of the size of the system of equations.

Assumption IV. The mesh of elements is constructed by repeatable patterns of smaller meshes in both directions.

Assumption IV has been inspired by the proportionality effect existing in the solution of original differential equations discussed in Section 2.1. Of course, to use such a proportionality property another assumption is needed

Assumption V. The numerical solution inherits the proportionality property form the governing differential equations.

We shall show that in order to employ assumption V, the numerical solution must be performed in a spectral form. Nevertheless, we do not expect that the proportionality values in each spectrum be equal to that of the original differential equation because of the approximation involved. This effect is usually referred to as dispersion and has been studied by many authors [19-26].

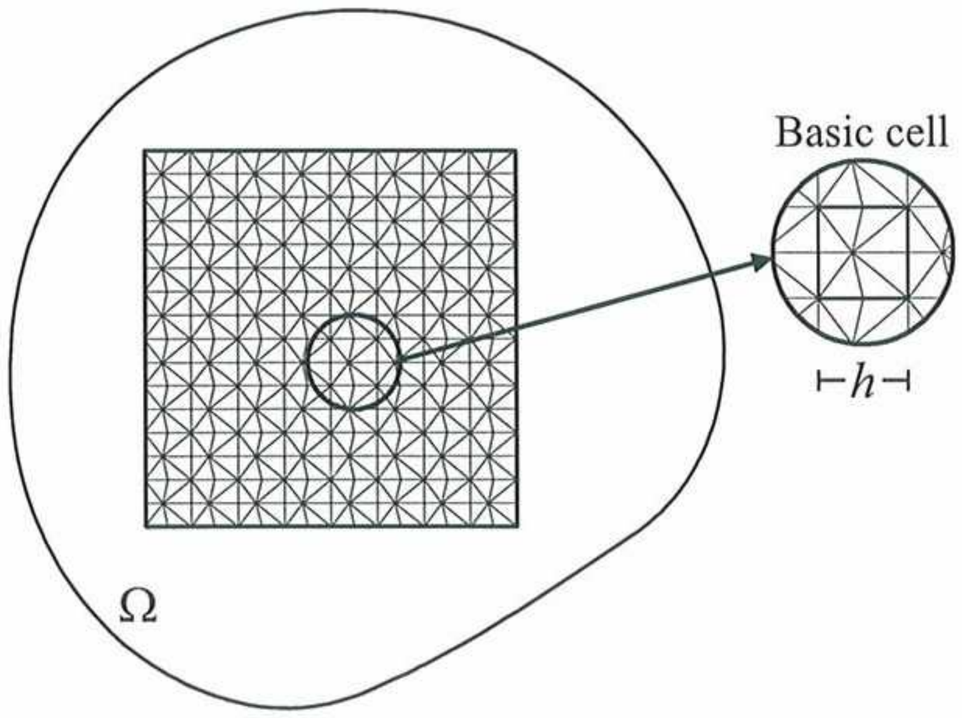

Figure 1. Grids with repeatable pattern constructed for unbounded domains, (a) a sample of mesh constructed, (b) degrees of freedoms in nearby nodes of a cell is written in terms of the those inside L-shape area.

Now a large mesh with repeatable pattern is considered. An example of such a mesh is illustrated in Figure 1-a. We shall refer to a unit of the repeating pattern as a "cell". Assembly of the coefficient matrix $\mathbf{K}_d$ in (28-b) may be performed first by assembly of the elements contributions at cell level and again assembly of similar units of the resulting sub-coefficient matrices. Note that the equilibrium equations at cell level pertaining to inner nodes should be condensed. Thus the remaining parts to be assembled with other cells are those pertaining to edge and corner nodes.

The final coefficient matrix can be schematically partitioned as

$$\begin{bmatrix} \mathbf{K}_{BB} & \mathbf{K}_{BI} \\ \mathbf{K}_{BI}^{T} & \mathbf{K}_{II} \end{bmatrix} \cdot \begin{Bmatrix} \bar{\mathbf{u}}_B \\ \bar{\mathbf{u}}_I \end{Bmatrix} = \begin{Bmatrix} \mathbf{f}_t \\ \mathbf{0} \end{Bmatrix} \tag{29}$$

In which B and I in subscripts denote the partitions pertaining to boundary nodes and those inside the domain (at interfaces of the cells) respectively. We temporarily leave the boundary partitions and focus on the parts pertaining to the inside nodes. Treatment of the boundary nodes for satisfaction of the external forces comes after finding an appropriate spectral solution for dynamic equilibrium state of the inside nodes.

Now considering a group of connecting cells far from the boundaries, it can be realized that the corresponding rows of the coefficient matrix in (29) are of similar form with repeated sequence. Smallest set of such rows of the matrix is constructed for nodes in L-shape shaded gray area in Figure 1-b.

The set of equations pertaining to shaded gray area in Figure 1-b can be represented by following compact form

$$\mathbf{k}_{ii}\bar{\mathbf{u}}_i + \mathbf{k}_{ij}\bar{\mathbf{u}}_j = \mathbf{0} \tag{30}$$

in which $\mathbf{k}_{ii}$ denotes the part of the coefficient matrix associated with DOFs of the nodes inside L-shape area, represented by $\bar{\mathbf{u}}_i$, and $\mathbf{k}_{ij}$ denotes the part associated with DOFs of the surrounding nodes, represented by $\bar{\mathbf{u}}_j$, contributing to equilibrium equations of the first set. In Figure 1-b, for instance, DOFs of nodes 1 to 3 are represented by $\bar{\mathbf{u}}_i$ and DOFs of nodes 4 to 21 are represented by $\bar{\mathbf{u}}_j$.

Now we apply the proportionality property as

$$\mathbf{u}_h^s(x+mL_x, y+nL_y) = \mu_1^m \mu_2^n \mathbf{u}_h^s(x,y) \tag{31}$$

Where L_x and L_y are cell dimensions along x and y, μ_1 and μ_2 are proportionality values which should be determined in a consistent manner. Superscript s is used for denoting spectral value of the function in a new space to be defined later. In above expression interpolated field of the unknowns (viz. Eqn. (23)) are used and clearly the same relation is valid for node values.

REMARK 2. The reader may note that similarity in rows of the coefficient matrix has roots in the type of the differential equation. In fact differential equation with constant coefficient has the property in differential length scale, i.e. the form is similar for all differential volumes. Similarity property of the equations and repeatability of the mesh pattern leads to sequential similarity effect in the coefficient matrix since the coefficient matrix is in fact the result of integration of the differential equation. The similarity effect in the coefficient matrix may also be seen even when the material properties vary periodically with period length of the mesh pattern. In that case the differential equation does not show such an effect. Nevertheless, as long as the coefficient matrix shows similarity effect, the proportionality is still applicable. This is another appealing effect of this approach which leads to solution of unbounded domain with repeatable material properties.
□

We use (31) in order to relate the values of nodes represented by $\bar{\mathbf{u}}_j$ to the values of nodes represented by $\bar{\mathbf{u}}_i$. For instance in Figure 1-b, following relations are used for a scalar wave problem

$$\bar{u}_{14} = \mu_1 \bar{u}_1 \quad , \quad \bar{u}_{12} = \mu_1^{-1} \bar{u}_1$$

$$\bar{u}_{19} = \mu_2 \bar{u}_1 \, , \quad \bar{u}_6 = \mu_2^{-1} \bar{u}_1$$

$$\bar{u}_{13} = \mu_1^{-1} \bar{u}_2 \, , \quad \bar{u}_{10} = \mu_2^{-1} \bar{u}_3$$

$$\bar{u}_4 = \mu_1^{-1}\mu_2^{-1} \bar{u}_1 \, , \quad \bar{u}_8 = \mu_1 \mu_2^{-1} \bar{u}_1 \, , \quad \bar{u}_{17} = \mu_1^{-1} \mu_2 \bar{u}_1 \, , \quad \bar{u}_{21} = \mu_1 \mu_2 \bar{u}_1 \tag{32-a}$$

and so forth. All relations may be written in a matrix form as

$$\bar{\mathbf{u}}_j^s = \mathbf{T}_{(\mu_1,\mu_2)} \bar{\mathbf{u}}_i^s \tag{32-b}$$

Substituting (32) in (30) leads to following matrix equation

$$\mathbf{Q}_{(\mu_1,\mu_2)}\overline{\mathbf{u}}_i^s = \mathbf{0} \tag{33}$$

In which

$$\mathbf{Q}_{(\mu_1,\mu_2)} = \mathbf{k}_{ii} + \mathbf{k}_{ij}\mathbf{T}_{(\mu_1,\mu_2)} \tag{34}$$

Equation (33) states that $\overline{\mathbf{u}}_i^s$ should be defined in terms of null space bases of $\mathbf{Q}$ when the determinant of $\mathbf{Q}$ is set to be zero

$$\left|\mathbf{Q}_{(\mu_1,\mu_2)}\right| = f(\mu_1,\mu_2) = 0 \tag{35}$$

Equation (35) serves as a characteristic equation as the one in (10). Two unknowns, μ_1 and μ_2, appear in one equation and thus one may be evaluated in terms of another

$$\mu_2 = g(\mu_1) \tag{36}$$

In a numerical solution one may choose a value for μ_1 and evaluate μ_2 form the characteristic equation (35). In choosing appropriate values for the proportionality parameters the decay and radiation condition must be kept in mind. In view of relations (18) we choose $\Re(\mu_1).\Im(\mu_1)<0$, and $\Re(\mu_2).\Im(\mu_2)<0$ to strictly satisfy the radiation condition (the reader may note that even positive sign of such products might be interpreted as radiation condition but the negative sign rigorously enforces this condition).

REMARK 3. Radiation conditions $\Re(\mu_1).\Im(\mu_1)<0$ and $\Re(\mu_2).\Im(\mu_2)<0$ are written for one cell. The physical interpretation of using these conditions for single cell is that the cell is enforced to transmit the information from one corner to other corners. When this applied for all cells the directional transmission over the whole domain is assured. It is worthwhile to note that although this leads to satisfaction of the radiation condition over a group of $m\times n$ cells, the same result could not be taken by considering $\Re(\mu_1^m).\Im(\mu_1^m)<0$ and $\Re(\mu_2^n).\Im(\mu_2^n)<0$. This is because when μ_1 and μ_2 are chosen so that $\Re(\mu_1).\Im(\mu_1)<0$ and $\Re(\mu_2).\Im(\mu_2)<0$ then, depending on exponents m and n, μ_1^m and μ_2^n may not show the same properties.

□

REMARK 4. In view of Remarks 1 and 3 it is seen that the dimensions of the cell play an important role in enforcement of the radiation condition. Considering the periodic lengths L_x and L_y as the cell dimensions, it can be concluded that in order to use $\Re(\mu_1).\Im(\mu_1)<0$ and $\Re(\mu_2).\Im(\mu_2)<0$, the cell dimensions must be less than a quarter of the associated wave lengths. In practice the cell dimensions are considered smaller than this limiting value.

□

The following function is then defined

$$\mu_2 = h(\mu_1) \qquad h = \left\{ g \;\middle|\; |g(\mu_1)| \le 1, |\mu_1| \le 1,\ \Re(g).\Im(g) < 0,\ \Re(\mu_1).\Im(\mu_1) < 0 \right\} \tag{37}$$

Generally, several relations like (37) exist since characteristic equation (35) possesses several roots for a given μ_1. Therefore

$$(\mu_2)_k = h_k(\mu_1) \tag{38}$$

Now supposing that $\boldsymbol{\phi}_{(\mu_1)}$ belongs to the null space of $\mathbf{Q}$, it may be observed that the nontrivial solution of (33) is

$$\bar{\mathbf{u}}_i^s = \boldsymbol{\phi}_{(\mu_1)} \tag{39}$$

Therefore the finite element solution for the set of nodes i may be written as

$$\bar{\mathbf{u}}_i = \int \left(\sum_k c_{k\,(\mu_1)} \boldsymbol{\phi}_{k(\mu_1)} \right) d\mu_1 \tag{40}$$

Where integration is taken over all feasible values of μ_1. We note that the vectors $\boldsymbol{\phi}_{k(\mu_1)}$ are normalized with respect to their lengths. In Equation (40) coefficients $c_{k\,(\mu_1)}$ are to be determined from boundary conditions at $x = 0$ or $y = 0$.

The number of inner summation in (40) is dependent on the number of $\boldsymbol{\phi}_{k\,(\mu_1)}$ for which μ_1 and μ_2 satisfy (37) and may vary when μ_1 takes different values.

Based on above details for selection of proportionality factors and associated vectors, in view of the last two conditions of (37) integral of (40) is written as

$$\bar{\mathbf{u}}_i = \int_{\frac{\pi}{2}}^{\pi} \int_{\varepsilon}^{1-\varepsilon} \left(\sum_k c_{k\,(\mu_1)} \boldsymbol{\phi}_{k(\mu_1)} \right) r dr d\theta + \int_{\frac{3\pi}{2}}^{2\pi} \int_{\varepsilon}^{1-\varepsilon} \left(\sum_k c_{k\,(\mu_1)} \boldsymbol{\phi}_{k(\mu_1)} \right) r dr d\theta \quad , \quad \mu_1 = re^{i\theta} \tag{43}$$

over the second and forth quadrants of the unit-radius circle of the Gaussian plane. In above integrals ε is chosen as a very small value ($\varepsilon = 10^{-5}$ in this study).

It may be noticed that, generally, in solution of characteristic equation (35) either μ_2 or μ_1 may be obtained in terms of the other one. Hence, it seems logical to perform both calculations and then modify (43) as

$$\bar{\mathbf{u}}_i = \sum_{n=1}^{2} \left\{ \int_{\frac{\pi}{2}}^{\pi} \int_{\varepsilon}^{1-\varepsilon} \left(\sum_k c^n_{k\,(\mu_n)} \boldsymbol{\phi}^n_{k(\mu_n)} \right) r_n dr_n d\theta_n + \int_{\frac{3\pi}{2}}^{2\pi} \int_{\varepsilon}^{1-\varepsilon} \left(\sum_k c^n_{k\,(\mu_n)} \boldsymbol{\phi}^n_{k(\mu_n)} \right) r_n dr_n d\theta_n \right\} , \mu_1 = r_1 e^{i\theta_1} , \mu_2 = r_2 e^{i\theta_2} \tag{44}$$

The integrations in (44) are to be taken numerically by using an appropriate Gauss quadrature rule. Therefore the integrals can be replaced by summation sings. The weights for quadrature points and corresponding $_n$ may be combined and considered as a part of coefficients of $c^n_{k\,(\mu_n)}$. Therefore one can write

$$\bar{\mathbf{u}}_i = \sum_{n=1}^{2} \sum_{\theta} \sum_{r} \sum_{k} C^n_{k(\mu_n)} \boldsymbol{\phi}^n_{k(\mu_n)} \tag{45}$$

In which $C^n_{k(\mu_n)}$ represents the combined coefficients. For simplicity all summations are shown symbolically while keeping in mind their limits

$$\bar{\mathbf{u}}_i = \sum C^n_{k(\mu_n)} \boldsymbol{\phi}^n_{k(\mu_n)} \;, \quad \mu_n = r_n e^{i\theta_n} \quad n = 1,2 \,, \quad \theta \in \{[0, \pi/2] \cup [3\pi/2, 2\pi]\} \;, \quad r \in (0,1) \tag{46}$$

Supposing that the coefficient values $C^n_{k(\mu_n)}$ are available we construct the finite element solution $\bar{\mathbf{u}}$ for the whole domain through defining characteristic vector $\mathbf{w}^n_{k(\mu_n)}$ from its smallest subset, i.e. $\boldsymbol{\phi}^n_{k(\mu_n)}$, using a transformation matrix like $\mathbf{T}'^{\,n}_{(\mu_n, h_k(\mu_n))}$ containing proportionality factors

$$\mathbf{w}^n_{k(\mu_n)} = \mathbf{T}'^{\,n}_{(\mu_n, h_k(\mu_n))} \boldsymbol{\phi}^n_{k(\mu_n)} \tag{47}$$

Clearly the dimension of $\mathbf{w}$ depends upon the number of cells considered along the two axes. The finite element solution is then obtained for the domain selected by $\mathbf{w}$ as

$$\bar{\mathbf{u}} = \sum C^n_{k(\mu_n)} \mathbf{w}^n_{k(\mu_n)} \tag{48}$$

We note that $\bar{\mathbf{u}}$ consists of both $\bar{\mathbf{u}}_I$ and $\bar{\mathbf{u}}_B$ in equation (29).

Now the question regarding the values of coefficients, $C^n_{k(\mu_n)}$, must be answered. For satisfying the Neumann/Dirichlet boundary conditions we shall start with the Dirichlet ones and then generalize the formulation to mixed boundary conditions which will include the Neumann ones.

1. *Dirichlet boundary condition:* Supposing that a set of prescribed nodal values as $\bar{\mathbf{u}}_B$ is available we need to satisfy $\bar{\mathbf{u}}\big|_{\Gamma_u} = \bar{\mathbf{u}}_B$ as essential boundary conditions. This means that

$$\left[\sum C^n_{k(\mu_n)} \mathbf{w}^n_{k(\mu_n)}\right]_{\Gamma_u} = \bar{\mathbf{u}}_B \tag{49}$$

or

$$\sum C^n_{k(\mu_n)} \mathbf{v}^n_{k(\mu_n)} = \bar{\mathbf{u}}_B \tag{50}$$

In which $\mathbf{v}^n_{k(\mu_n)}$ is a vector containing components of $\mathbf{w}^n_{k(\mu_n)}$ that fall on Γ_u and can be defined by components of $\boldsymbol{\phi}^n_{k(\mu_n)}$ using a suitable transformation matrix

$$\mathbf{v}^n_{k(\mu_n)} = \mathbf{T}^n_0 \boldsymbol{\phi}^n_{k(\mu_n)} \tag{51}$$

Here $\mathbf{T}^n_0$ contains the proportionality factors, μ_1 and μ_2, and selects the nodal values of $\boldsymbol{\phi}^n_{k(\mu_n)}$ for boundaries.

Now we assume that the coefficient value associated with a value for μ_n is proportional to the projection of $\bar{\mathbf{u}}_B$ on $\mathbf{v}^n_{k(\mu_n)}$. Such an assumption, which is consistent with conventional mathematical transformations, is applied in its general form as

$$C^n_{k(\mu_n)} = \left(\mathbf{v}^n_{k(\mu_n)}\right)^T \mathbf{R}\bar{\mathbf{u}}_B \tag{52}$$

Where $\mathbf{R}$ is a matrix assumed to be independent of μ_n and to be determined so that Equation (52) holds for all values of μ_n. We note that arrays in relation (52) are generally of infinite number of components since infinite number of boundary nodes exist along $x=0$ and $y=0$. For a computable solution, one needs to truncate the arrays. Truncation of the arrays is performed based on the largeness of the solution area and the accuracy required.

To evaluate $\mathbf{R}$ we substitute (52) in (50) to obtain

$$\left[\sum \mathbf{v}^n_{k(\mu_n)}\left(\mathbf{v}^n_{k(\mu_n)}\right)^T \mathbf{R}\right]\bar{\mathbf{u}}_B = \bar{\mathbf{u}}_B \tag{53}$$

Since $\mathbf{R}$ is assumed to be independent of μ_n, it can be taken out of the summation sign

$$\left[\sum \mathbf{v}^n_{k(\mu_n)}\left(\mathbf{v}^n_{k(\mu_n)}\right)^T\right]\mathbf{R}\bar{\mathbf{u}}_B = \bar{\mathbf{u}}_B \tag{54}$$

Above relation implies that

$$\mathbf{R} = \left[\sum \mathbf{v}^n_{k(\mu_n)}\left(\mathbf{v}^n_{k(\mu_n)}\right)^T\right]^{-1} \tag{55}$$

The number of integration points required is dependent on the number of prescribed values, i.e. the length of $\bar{\mathbf{u}}_B$. The reader will note that vectors $\mathbf{v}_k$ are not orthogonal and thus increasing the number of integration points helps to obtain a full rank matrix.

Having found matrix $\mathbf{R}$, the finite element solution is evaluated from (48) as

$$\bar{\mathbf{u}} = \sum\left(\left(\mathbf{v}^n_{k(\mu_n)}\right)^T \mathbf{R}\bar{\mathbf{u}}_B\right)\mathbf{w}^n_{k(\mu_n)} \tag{56}$$

or

$$\bar{\mathbf{u}} = \left(\sum \mathbf{w}^n_{k(\mu_n)}\left(\mathbf{v}^n_{k(\mu_n)}\right)^T\right)\mathbf{R}\bar{\mathbf{u}}_B \tag{57}$$

The solution corresponds to the homogenous part of the solution to integral equation (29) with presence of prescribed boundary values for the main function, i.e. when $\bar{\mathbf{u}}_B$ is prescribed instead of $\mathbf{f}_t$.

2. Mixed boundary conditions In order to find general relation between nodal resultant of tractions $\mathbf{f}_t$ and corresponding nodal values of the function $\bar{\mathbf{u}}_B$ one can evaluate the nodal resultants due to finite element field presented in (57). To this end, the first row of matrix equation (29) is rewritten

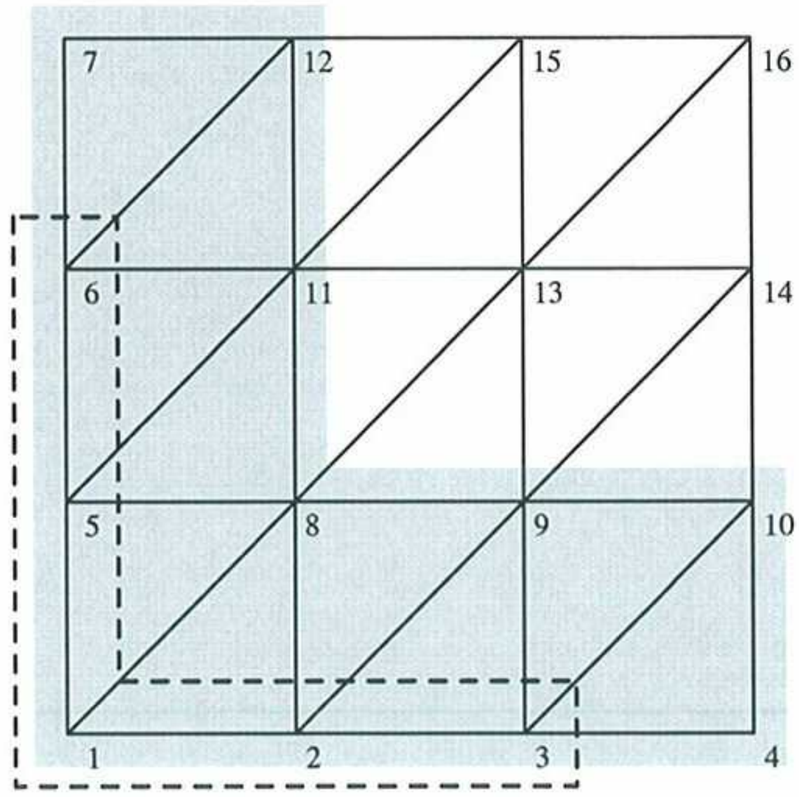

Figure 2. Nodes and cells contributing to tractions at a boundary of a sample mesh (shaded gray area). Nodes 1,2,3,5 and 6 are those for which the Neumann conditions are to be satisfied and nodes 4,7,8,9,10,11 and 12 represent the nodes which contribute to nodal forces at the former set.

$$\mathbf{K}_{BB}\bar{\mathbf{u}}_B + \mathbf{K}_{BI}\bar{\mathbf{u}}_I = \mathbf{f}_t \tag{58}$$

It should be noted that just a small part of $\bar{\mathbf{u}}_I$, including the first set of inner nodes, contributes to $\mathbf{f}_t$ (see Figure 2). Equation (58) may be written as

$$\mathbf{K}_{bnd}\bar{\mathbf{u}}' = \mathbf{f}_t \tag{59}$$

In which $\bar{\mathbf{u}}'$ is the union of $\bar{\mathbf{u}}_B$ and the part of $\bar{\mathbf{u}}_I$ contributing to $\mathbf{f}_t$, and $\mathbf{K}_{bnd}$ is corresponding rectangular coefficient matrix, arranged from $\mathbf{K}_{BB}$ and $\mathbf{K}_{BI}$, which is the assembly of coefficient matrices at the boundary. For instance for simple mesh pattern in Figure 2, $\bar{\mathbf{u}}_B$ represents the DOFs of nodes 1,2,3,5 and 6, and $\bar{\mathbf{u}}_I$ represents the DOFs of nodes 4,7,8,9,10,11 and 12.

In order to construct $\bar{\mathbf{u}}'$ in terms of $\bar{\mathbf{u}}_B$, in (57) vector $\mathbf{w}^n_{k(\mu_n)}$ is replaced with a suitable one

$$\bar{\mathbf{u}}' = \left(\sum \mathbf{v}'^{\,n}_{k(\mu_n)} \left(\mathbf{v}^n_{k(\mu_n)}\right)^T\right)\mathbf{R}\bar{\mathbf{u}}_B \tag{60}$$

In above relation $\mathbf{v}'^{\,n}_{k(\mu_n)}$ is a vector the components of which are subset of components of $\mathbf{w}^n_{k(\mu_n)}$ and corresponds to the sets of node contributing to boundary tractions (nodes 1 to 12 in Figure 2 for instance). Construction of $\mathbf{v}'^{\,n}_{k(\mu_n)}$ may be performed through defining a suitable transformation matrix as below

$$\mathbf{v}'^{\,n}_{k(\mu_n)} = \mathbf{T}'^{\,n}_0 \boldsymbol{\phi}^n_{k(\mu_n)} \tag{61}$$

Where $\mathbf{T}_0'^{\,n}$ contains the proportionality factors μ_1 and μ_2, and selects the nodal values of $\phi^n_{k(\mu_n)}$ at or near boundaries.

Now substitution of (60) in to (59) leads to

$$\mathbf{K}_{bnd}\left(\sum \mathbf{v}'^{\,n}_{k(\mu_n)}\left(\mathbf{v}^n_{k(\mu_n)}\right)^T\right)\mathbf{R}\bar{\mathbf{u}}_B = \mathbf{f}_t \tag{62}$$

Above equation relates the nodal resultants of traction and the corresponding nodal values of the main function. In a conventional form of notation

$$\mathbf{K}_0\bar{\mathbf{u}}_B = \mathbf{f}_t\ , \qquad \mathbf{K}_0 = \mathbf{K}_{bnd}\left(\sum \mathbf{v}'^{\,n}_{k(\mu_n)}\left(\mathbf{v}^n_{k(\mu_n)}\right)^T\right)\mathbf{R} \tag{63}$$

Where the so defined $\mathbf{K}_0$ plays the role of a condensed dynamic stiffness of the domain evaluated at nodes on $x=0$ and $y=0$. Clearly, matrix $\mathbf{K}_0$ is a complex matrix and its imaginary part is interpreted as a damping matrix due to dissipated energy via radiation.

It may be noticed that with Equation (63) in hand, one can consider pure Neumann conditions at $x=0$ and $y=0$ when $\mathbf{f}_t$ is known a priori and $\bar{\mathbf{u}}_B$ is a set of the unknowns. In that case, $\bar{\mathbf{u}}_B$ is evaluated from (63) and the rest of nodal values are calculated by (57).

REMARK 5. As an alternative way, especially for problems with pure Neumann conditions, one may start from (59) by replacing $\bar{\mathbf{u}}'$ with its equivalent series

$$\mathbf{K}_{bnd}\bar{\mathbf{u}}' = \mathbf{f}_t \quad , \quad \bar{\mathbf{u}}' = \sum C^n_{k(\mu_n)}\mathbf{v}'^{\,n}_{k(\mu_n)} \tag{65}$$

with $\mathbf{v}'^{\,n}_{k(\mu_n)}$ defined as (61). Analogous to (52), the coefficients may be assumed to be proportional to the projection of $\mathbf{K}_{bnd}\mathbf{v}'^{\,n}_{k(\mu_n)}$ on nodal tractions resultants $\mathbf{f}_t$. Therefore

$$C^n_{k(\mu_n)} = \left(\mathbf{K}_{bnd}\mathbf{v}'^{\,n}_{k(\mu_n)}\right)^T\mathbf{R}'\mathbf{f}_t \tag{66}$$

with $\mathbf{R}'$ being again a matrix assumed to be independent of μ_n and to be determined so that (66) holds for all values of μ_n. Following similar reasoning in (53) to (55) it can be concluded that

$$\mathbf{R}' = \left[\sum \mathbf{K}_{bnd}\mathbf{v}'^{\,n}_{k(\mu_n)}\left(\mathbf{K}_{bnd}\mathbf{v}'^{\,n}_{k(\mu_n)}\right)^T\right]^{-1} = \left[\mathbf{K}_{bnd}\left[\sum \mathbf{v}'^{\,n}_{k(\mu_n)}\left(\mathbf{v}'^{\,n}_{k(\mu_n)}\right)^T\right]\mathbf{K}^T_{bnd}\right]^{-1} \tag{67}$$

The finite element solution is then evaluated as

$$\bar{\mathbf{u}} = \left(\sum \mathbf{w}^n_{k(\mu_n)}\left(\mathbf{v}'^{\,n}_{k(\mu_n)}\right)^T\right)\mathbf{K}^T_{bnd}\mathbf{R}'\mathbf{f}_t \tag{68}$$

which is written in flexibility form. It is obvious that this form can also be employed for problems with mixed Dirichlet and Neumann conditions as what we saw in (63). Nevertheless, it is not easy

to show that the coefficient matrix in (68) is inverse of $\mathbf{K}_0$ in (63) but from uniqueness of the solution, however, it is expected that at least for the gradients both forms give similar results. In this report we employ the form given in (63).

□

Our experience in using relation (63) shows that $\mathbf{K}_0$ becomes ill-conditioned when a relatively large number of cells are used for satisfaction of the boundary conditions. In fact, the first signs of ill-condition effect appear in evaluation of $\mathbf{R}$ through relation (55). The expression inside the bracket in (55) becomes ill-conditioned due to round off errors occurring in evaluations of vector $\mathbf{v}^n_{k\,(\mu_n)}$.

From a computational mathematics stand of view, it is well understood that ill-condition effect is in close relation with the precision used for the computations. Therefore such an effect can be completely eliminated by increasing the precision. Nowadays, with available routines, it is possible to use any desirable precision.

Nevertheless, it may be appealing to use machine precision to take advantage of compatibility with other routines available for engineering computation. The reader is referred to Appendix A for possible way of treating the problem.

In the next section we shall give results for numerical solution of some scalar and elasticity wave problems.

4. NUMERICAL RESULTS

In this section we present numerical results for some benchmark problems. We shall try to evaluate the Green's functions, with definitions given in (3) and (4), for scalar and elasticity wave problems. It is well understood that any other wave problem can be solved by use of such fundamental solutions through superposition of the effects as is usually performed in boundary integral method.

We shall give discussion on the convergence of the solution in terms of the number of cells used along x and y axes as well as the number points used in Gaussian plane for summations required in the formulation.

An L_2 norm defined over a bounded area is used for convergence study. We define

$$\|\bar{\mathbf{u}}\| = \sqrt{\sum |\bar{u}_i|^2}$$

for nodal values of scalar wave problems and

$$\|\bar{\mathbf{u}}\| = \sqrt{\sum (|\bar{u}_i|^2 + |\bar{v}_i|^2)}$$

for nodal values of elastic wave problems. In above norms | . | denotes absolute values of the quantity noting that the nodal quantities can be complex values.

Example 1. As the first benchmark problem we consider the following scalar wave equation,

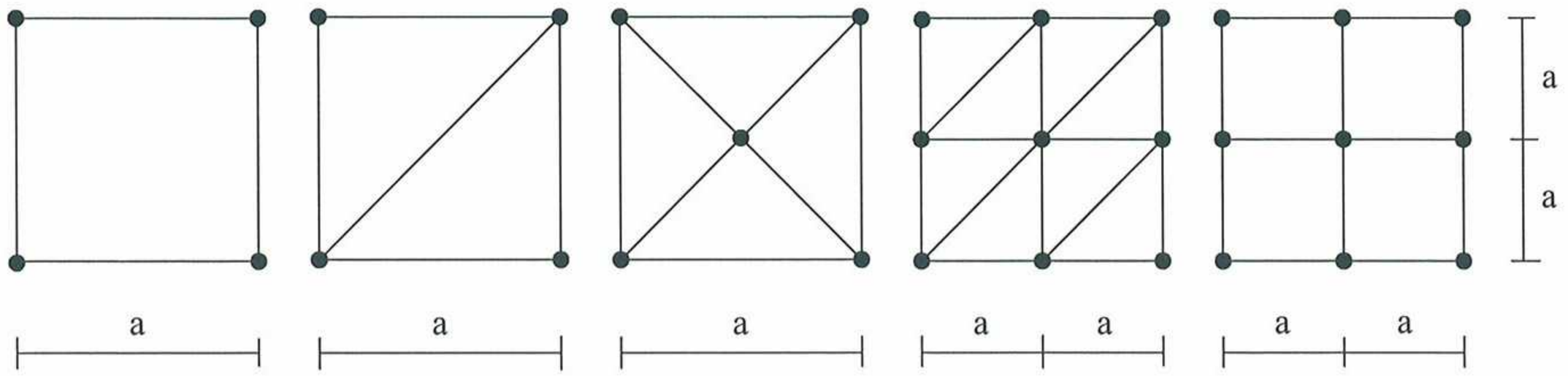

Figure 3. Patterns of cells used for numerical solutions, (a) four node quadrilateral element (b) regular pattern of three node triangular elements (c) Criss-Cross pattern of triangular elements (d) doubly arranged regular patterns of triangular elements (e) doubly arranged linear quadrilateral elements.

$$\frac{\partial^2 U}{\partial x^2}+\frac{\partial^2 U}{\partial y^2}-\frac{1}{c^2}\frac{\partial^2 U}{\partial t^2}=f(x,y,t)$$

in which c is the wave speed and $f(x,y,t)$ is the source term. The equation has numerous applications in physics and mechanics. The Green's function in frequency domain is obtained by assuming $f(x,y,t)=\delta(x)\delta(y)e^{i\omega t}$ and seeking for steady state solution as $U=ue^{i\omega t}$. In this example $\omega^2=3$ and $c=1$. The following partial differential equation is obtained.

$$\frac{\partial^2 u}{\partial x^2}+\frac{\partial^2 u}{\partial y^2}+\frac{\omega^2}{c^2}u=\delta(x)\delta(y) \qquad (x,y)\in\mathbb{R}\times\mathbb{R}$$

The homogenous part of the equation, known as Helmholtz equation, is in fact a special form of equation (20) with operator **S** being as (22), $k_x=k_y=1$ and also $\rho=1$. When the Laplace operator is written in a polar coordinate the exact solution of the differential equation may be found as

$$u=C_1H_0^2(\frac{\omega}{c}r)$$

with H_0^2 being Hankel function of second kind and $r=\sqrt{x^2+y^2}$. Coefficient C_1 is found by making balance between the gradients from the solution and those induced by source term near origin. As is seen the solution is singular and needs special treatment when is used in boundary integral method. However, when the solution is performed through finite element method the singularity effect disappears and the solution remain finite at origin. In order to use the proposed method, first we redefine the problem over a quarter of the full space with the following boundary conditions

$$\left.\frac{\partial u}{\partial y}\right|_{y=0}=0\ , \qquad \left.\frac{\partial u}{\partial x}\right|_{x=0}=0 \qquad (x,y)\in[0,\infty)\times[0,\infty)$$

We shall employ a series of meshes with basic repeated cells as shown in Figure 3. The solution for meshes constructed by cells of Figure 3-a-b-c can be found, in spectral form, by writing the proportionality relations for all nodes in terms of one node, e.g. node number one. The element dimensions in all cell patterns are considered as $a=b=0.25$. This reduces **Q** matrix in (34) to a scalar

similar to the characteristic equation (35) and therefore there will be no need for finding null space basis ϕ.

In order to give some insight to the forms of the characteristic equations resulted from using each basic cell of Figure 3-a and 3-c, we present them in Appendix B.

Figure 4 and 5 depict three dimensional and contour plots of the real and imaginary parts of the solutions obtained for the three finite element meshes. The exact solution is also shown in the same figure and has been cut at singularity point in order to be comparable with the finite element solution at the other parts of the domain. In these solutions 40 boundary cells are used along each axis to satisfy the boundary conditions which are of Neumann type with zero values except the corner node at origin. For integration over the Gaussian plane, see (46), 40 points are used along the radial and angular directions separately. It can be seen that the numerical solutions are in agreement with the exact solution.

It might also be interesting to know the effects of choosing a larger cell as a repeated basic one. The reader may notice that a basic cell like shown in Figure 3-d and 3-e can also be used as the basic cell. In that case matrix $\mathbf{Q}$ in (34) will be a 3×3 matrix since all nodal values, in spectral form, can be written in terms of values at nodes 1,2 and 3 in Figure 1-b. The vectors in null space of $\mathbf{Q}$ are of 3×1 dimension.

It can be seen that the larger the cell the higher is the order of the characteristic equation. In order to compare the results with the ones from smaller cell, 20 cells are used along each axis to satisfy the boundary conditions. The number of points for integration over Gaussian plane is the same as the one used for solution with smaller cells (cells in Figures 3-a and 3-b). The results are shown in Figure 6 which should be compared with Figures 4-a-b-c-d for real parts and Figures 5-a-b-c-d for imaginary parts.

To study the convergence of the solution, different numbers of integration points are used in a series of solutions. Figure 7 demonstrates the results. Note that the numbers given for integration points represent the number of points used along each direction in Gaussian plane, i.e. along and θ, and thus one point increase in the figure represents $2N+1$ increase in the total number of points used in each quadrant of the unit-radius circle. Forty cells are used along each axis for satisfaction of the boundary conditions and the norms are calculated over an area of 20×20 cells.

For linear quadrilateral elements excellent convergence is seen. Maximum difference between norm values for above 35 integration points is less than 0.0003% as is seen in Figure 7-a. For regular triangles, however, the convergence seems to be rather cumbersome. In this case, as Figure 7-b depicts, the difference between values of the norms is about 1.3%, for above 35 integration points, which is much higher than that of the previous case. Figure 7-c shows convergence of the solution when Criss-Cross pattern is used. The maximum difference between norm values for above 35 integration points is less than 0.0005% which is in the same order as obtained for linear quadrilaterals. One important observation is that in Figures 7-a and 7-c, as a rule of thumb, the minimum number of integration points is within the order of the number of cells used for satisfaction of boundary conditions along the x and y axes.

The reader may notice that although all cell patterns consist of linear elements, small differences are seen between the solutions and especially the convergences obtained. The sources for differences can be traced by counting the number of nodes within a wave length along different directions and noting

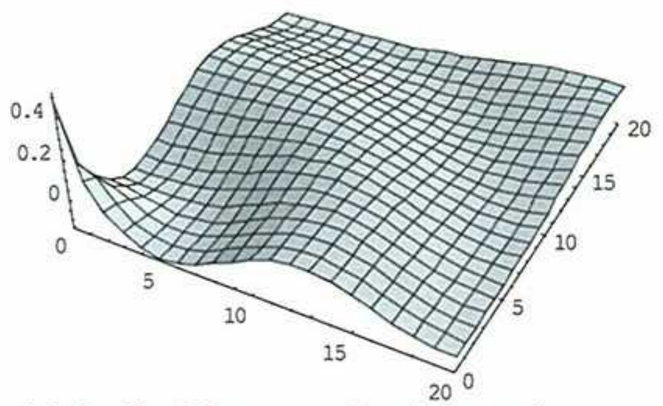

(a) Cell of four node element

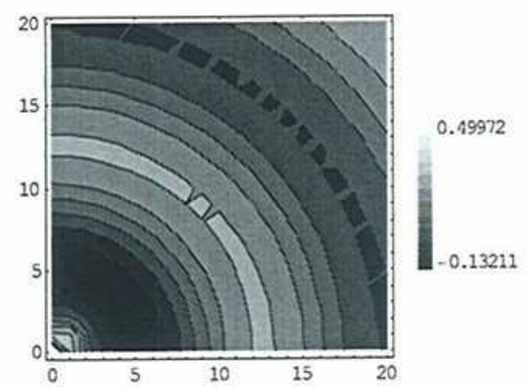

(b) Cell of four node element

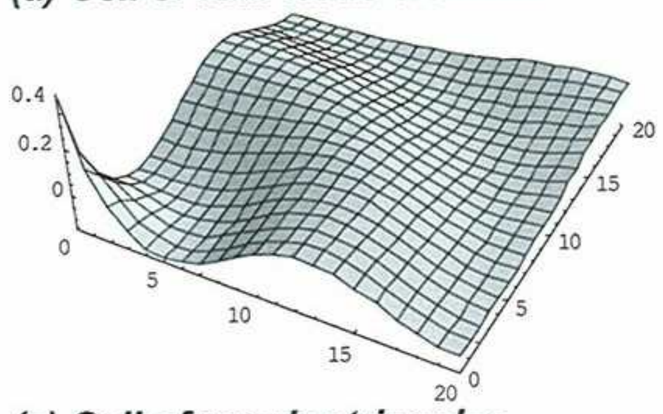

(c) Cell of regular triangles

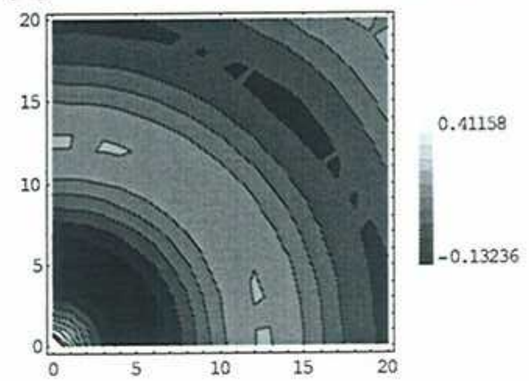

(d) Cell of regular triangles

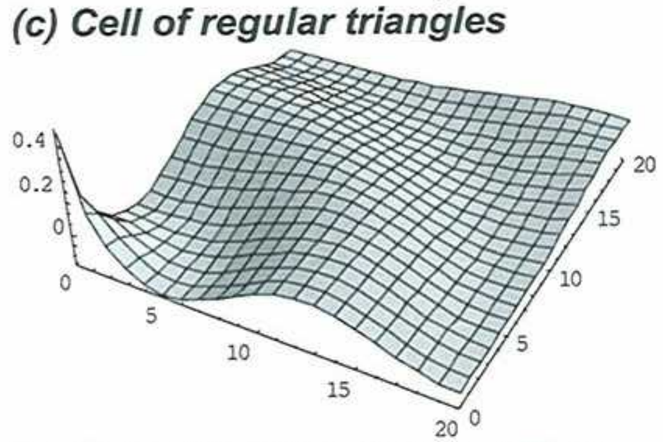

(e) Cell with Criss-Cross pattern

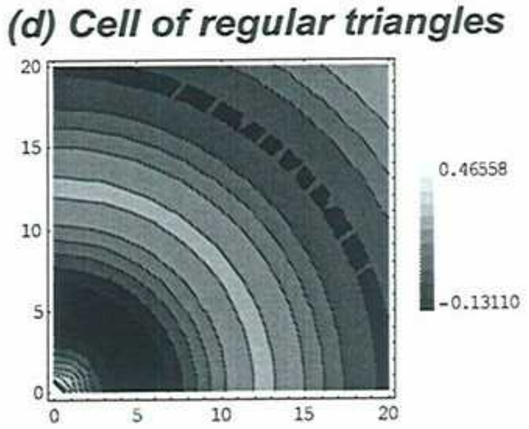

(f) Cell with Criss-Cross pattern

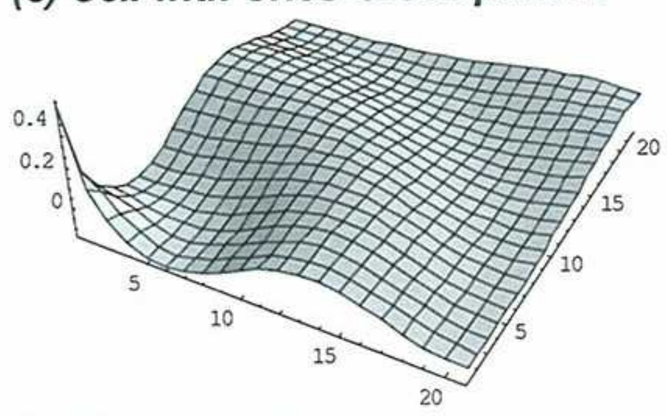

(g) Exact solution

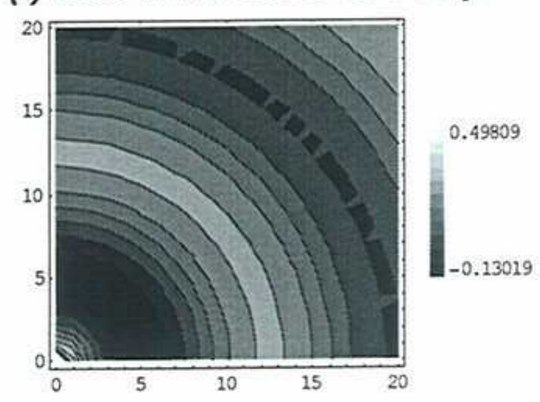

(h) Exact solution

Figure 4. The real parts of solutions in scalar wave problem. The numbers on x and y axes represent the number of cells used. Forty cells are used along each axis for satisfaction of the boundary conditions. The solutions are plotted over an area of 20 × 20 cells.

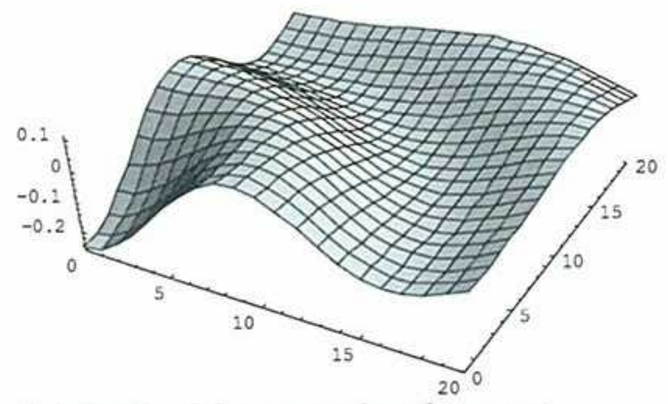

(a) Cell of four node element

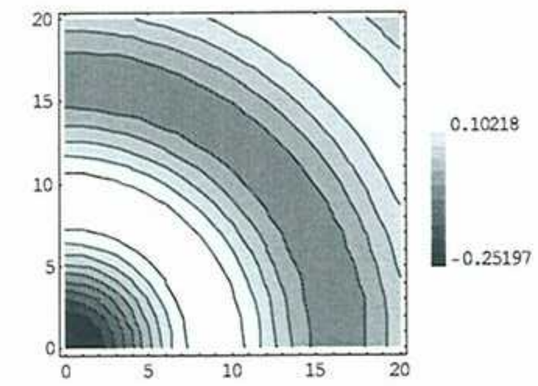

(b) Cell of four node element

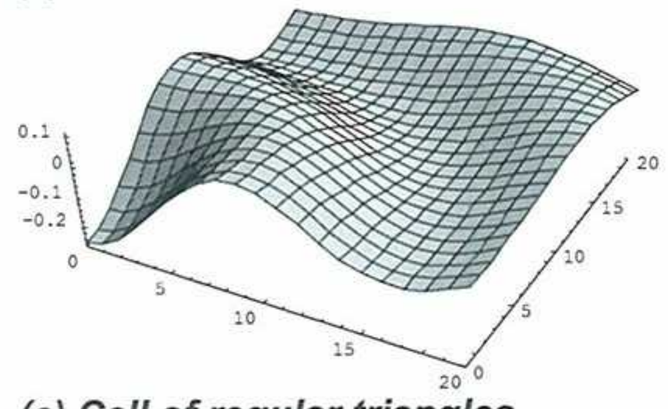

(c) Cell of regular triangles

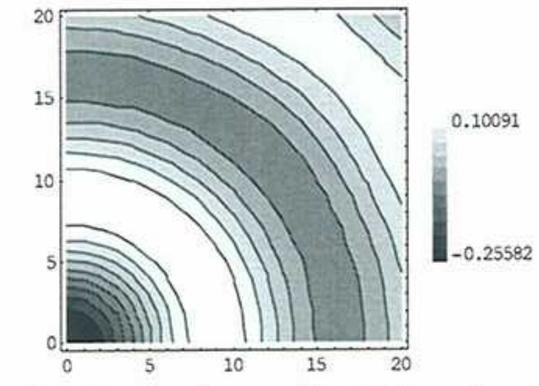

(d) Cell of regular triangles

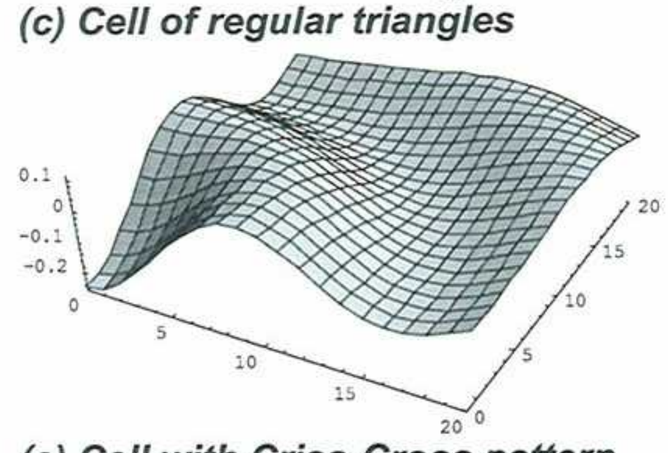

(e) Cell with Criss-Cross pattern

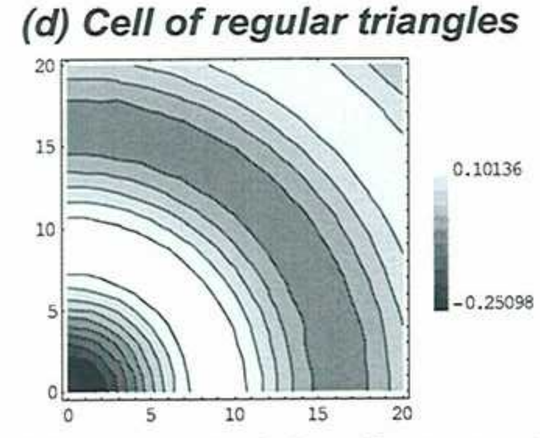

(f) Cell with Criss-Cross pattern

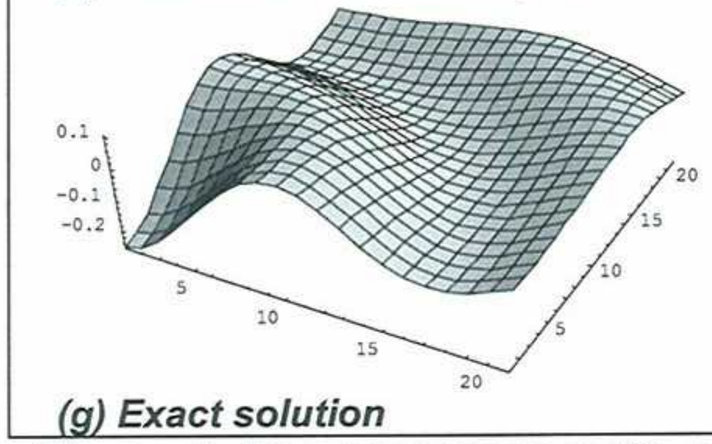

(g) Exact solution

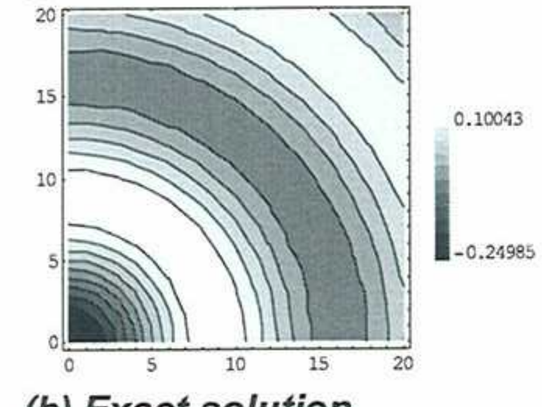

(h) Exact solution

Figure 5. The imaginary parts of solutions in scalar wave problem. The numbers on x and y axes represent the number of cells used. Forty cells are used along each axis for satisfaction of the boundary conditions. The solutions are plotted over an area of 20 × 20 cells.

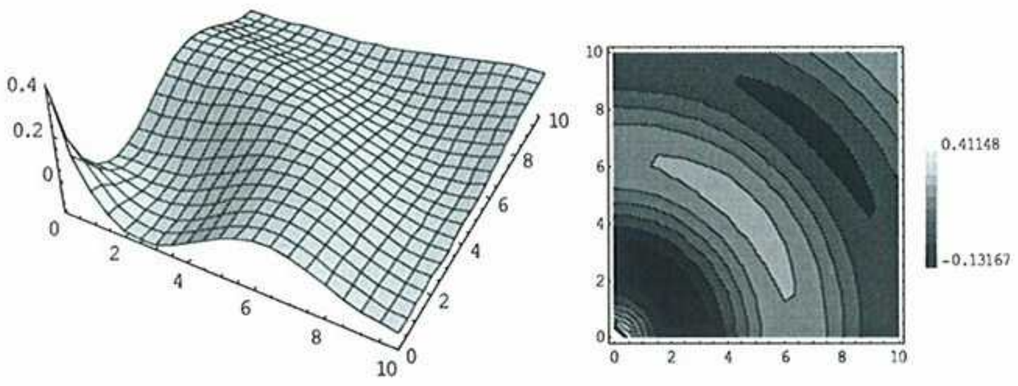

(a) Double regular triangles- $\Re(u)$

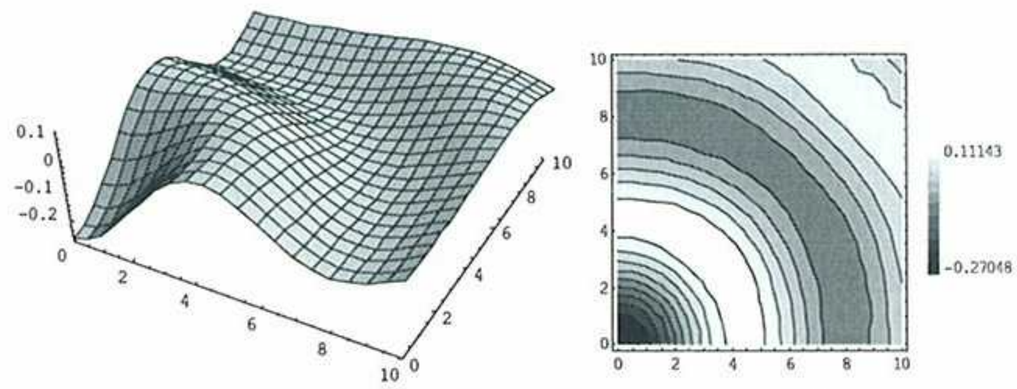

(b) Double regular triangles- $\Im(u)$

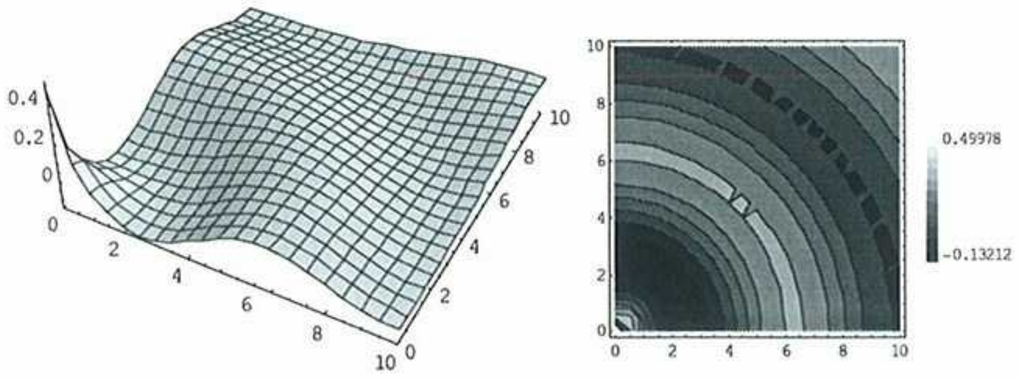

(c) Double quadrilaterals- $\Re(u)$

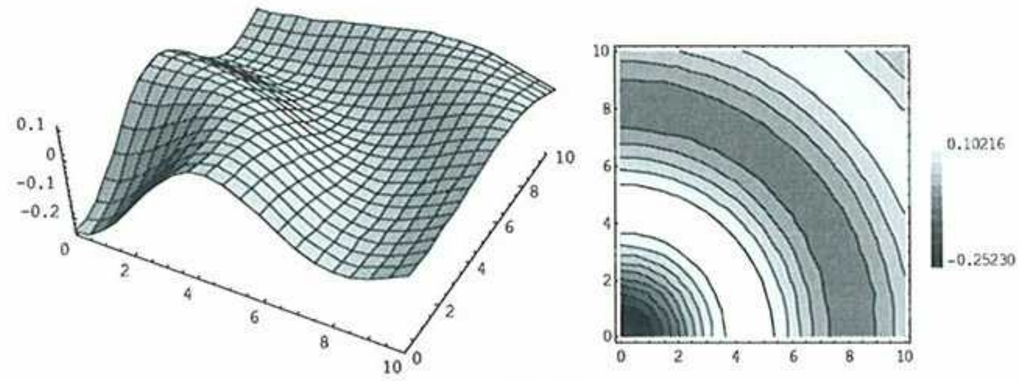

(d) Double quadrilaterals- $\Im(u)$

Figure 6. Three dimensional and contour plots for variation of the real and imaginary parts of the solutions in scalar wave problem. Twenty cells are used for satisfaction of the boundary conditions and the solution are plotted over an area of 10×10 cells; (a) and (b) solution using mesh with basic cell of doubly arranged regular pattern of triangles as Fig. 3-d, (c) and (d) solution using mesh with basic cell of doubly arranged bilinear elements as Fig. 3-e.

the interpolation used. Along x and y axes patterns of regular triangles and square quadrilaterals have similar number of nodes and similar interpolation order within a wave length. However one may notice that along $x = y$ axis the number of node per wave length differs from those along main axes and, although both types have similar node per wave length, the cells with regular triangles are of less order of interpolation compared with cells with linear quadrilaterals. In linear rectangular elements the interpolation is of quadratic order along the diagonal. Therefore it is expected that the performance of the regular triangular elements, as the pattern shown in Figure 3-c, be inferior to that of the square elements (see Figure 4-b and 4-c for real part of the solution). The effect of number of nodes per wave length and the associated interpolation, causing phase lead or error in direction of the wave propagated, is usually referred to as dispersion effect and has been studied by many scientists. For problems with Helmholtz equation the reader may refer to works by Ihlenburg and Babuška in [20, 21] or Babuška *et al* in [22-24] for example.

Apart from the general expectation from performances of different cells, it may be observed that, regarding the formulation used in this report and referring to the relations in (32-a), nodal values at two sides of a diagonal of a cell are proportional with a factor which is a cross product of the two proportionality values μ_1 and μ_2. This effect is consistent with variation of shape functions in four node quadrilateral elements which is of quadratic form, i.e. cross product of local normalized coordinates inside of a bilinear element, and of course is not consistent with the interpolation inside regular triangular patterns. This inconsistency for regular patterns has a pronounce effect when either of integrant variables μ_1 and μ_2 are quite small and thus it is logical to expect that the convergence of the solution be rather cumbersome with respect to the number of integration points.

Sources mentioned above for the different behaviors indicate that patterns similar to Figure 3-b lead to a sort of directional behavior in the solution. The directional behavior of the solution is much

pronounced in elastic wave problems which are to be addressed in forthcoming examples. However, when one uses Criss-Cross pattern of triangles (see Figure 3-c) the problem of directional node per wave length is alleviated by adding a node along the diagonal directions. Moreover, the problem of interpolation is also reduced since there is no explicit relation inside the cell between the two nodal values at the ends of diagonals. This is mainly because that the shape function associated with the middle node acts as a sort of bubble function and thus alleviates the excessive stiffness of the cell seen in the previous case. The results given in Figures 4-e-f and 5-e-f for distribution of real and imaginary parts of the solution and the ones in Figure 7-c for convergence of the solution show that Criss-Cross pattern produces quite similar results to those obtained form use of bilinear quadrilateral elements.

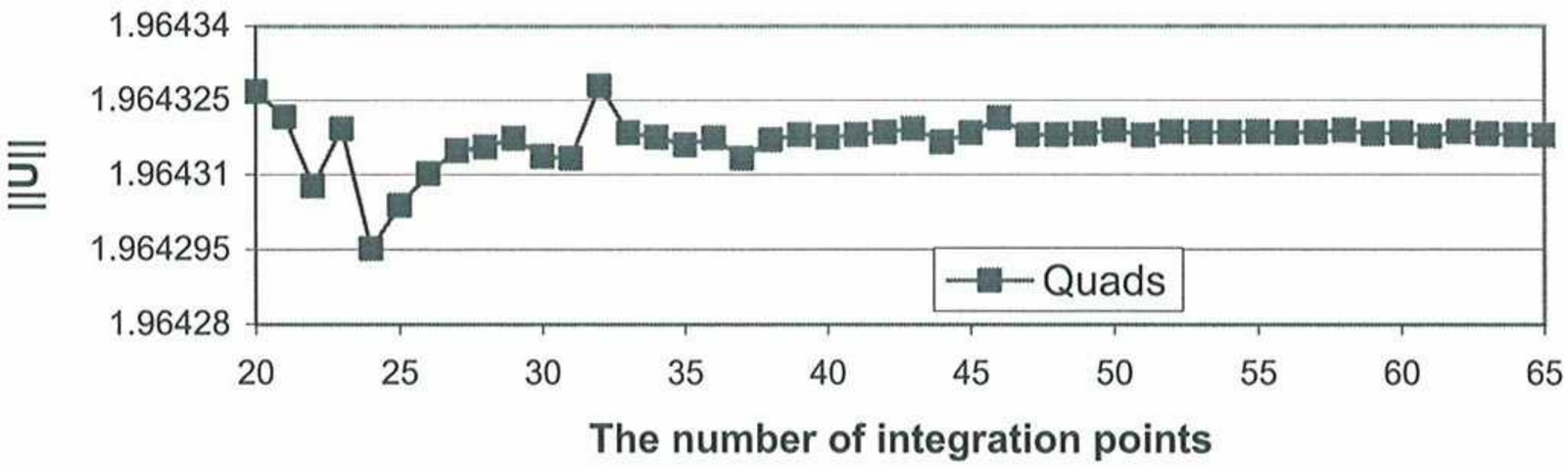

(a)

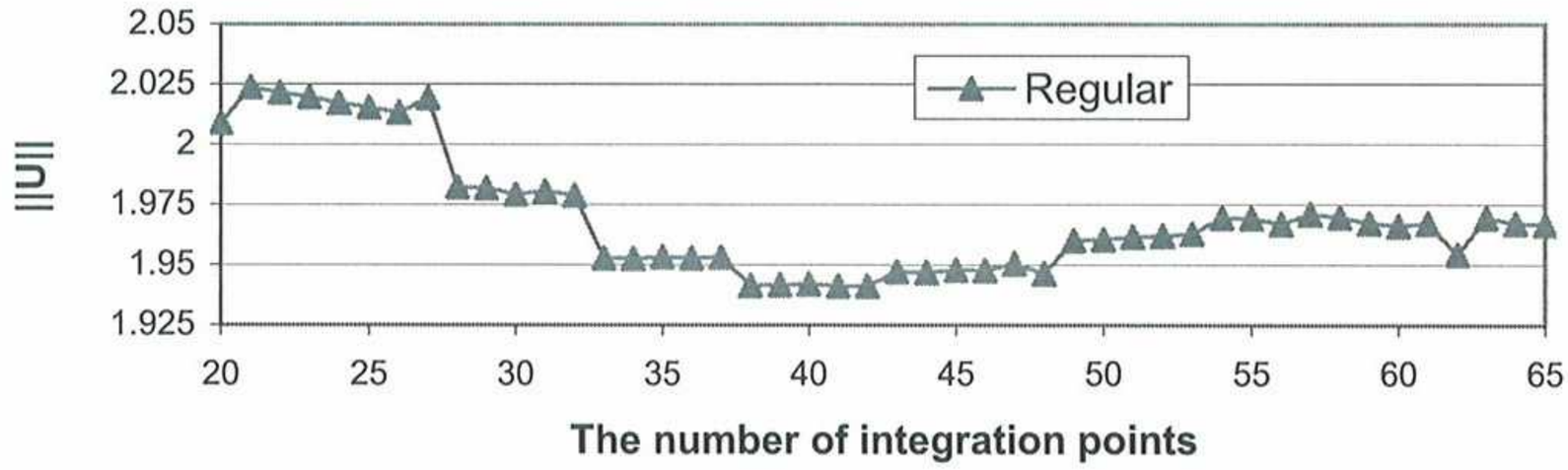

(b)

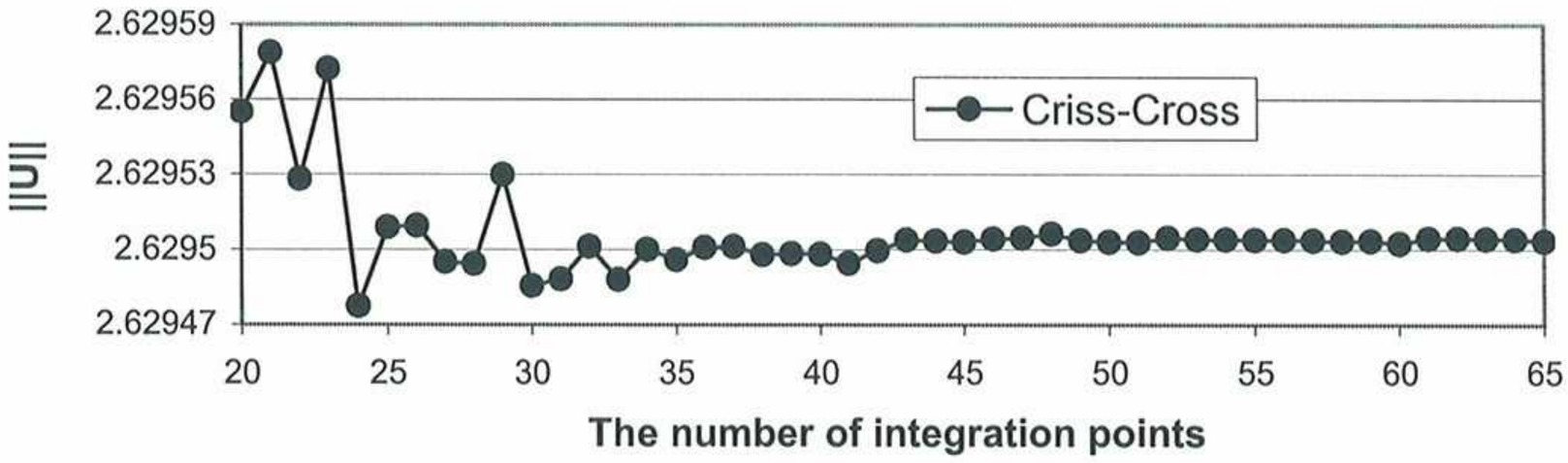

(c)

Figure 7. Variation of L_2 norms of the solution, for scalar wave problem, versus the number of integration points used for different patterns of cells. The norms are calculated over an area of 20×20 cells and 40 cells are used along each axis for satisfaction of the boundary conditions.

It should be noted that using Criss-Cross pattern or larger cell of regular pattern instead of single regular pattern just reduces the effects of inconsistencies between the interpolation and the formulation

given in this report. Different behavior is still seen along diagonal direction in Figures 6-a-b. Note that the effects of dispersion may still remain even in the case of using quadrilateral elements. Some remedies for reduction of the dispersion, such as the ones given in [25] and [26], may also be sought and implemented in the finite element formulation given here which of course are beyond of the scopes of this report. However, the method proposed in this report may be employed for studies in dispersion analysis in unbounded domains without need of using artificial boundary conditions..

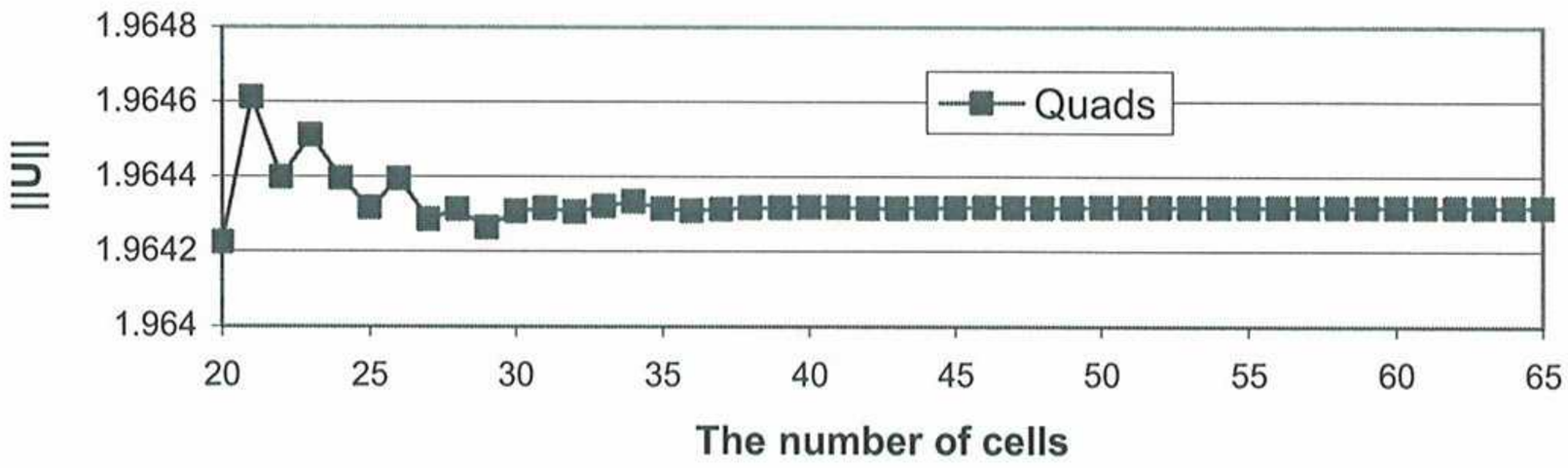

Figure 8. Variation of L_2 norms of the solution, for scalar wave problem, versus the number of cells used for satisfaction of boundary conditions. The norms are calculated over an area of 20×20 cells and 40 points are used for integrations.

All results so far shown for this example were taken over an area with fixed number of cells along x and y axes. Figure 8 shows convergence of the solution with respect to the number of cells used along the two axes. Here again for evaluation of the norms an area of 20×20 cells is used. Linear quadrilateral elements are used in the study. The figure clearly shows the method proposed in this report is convergent with respect to the number of cells for boundary conditions.

As final results for this example we present the distributions of the real and imaginary parts of the solution when 100 cells are used along each axis. Three dimensional plots of the numerical and exact solutions are presented in Figure 9. The results obtained with procedure explained in Appendix A using machine precision. The figure shows that the method proposed is capable of giving numerical solution to a large area, with respect to the wave length, of an unbounded domain.

Example 2. The problem of the first example is solved again with orthotropic material $k_x = 1$ and $k_y = 4$. The differential equation takes the following form

$$\frac{\partial^2 u}{\partial x^2} + 4\frac{\partial^2 u}{\partial y^2} + \frac{\omega^2}{c^2}u = \delta(x)\delta(y) \quad , \quad \omega^2 = 3, \quad c = 1 \; , \quad x \geq 0 \; , \; y \geq 0 \; , \quad \left.\frac{\partial u}{\partial y}\right|_{y=0} = 0 \quad \text{and} \quad \left.\frac{\partial u}{\partial x}\right|_{x=0} = 0$$

The exact solution may be obtained by suitable mapping as $y' = 2y$ and using the same form as given in the first example with $r = \sqrt{x^2 + 4y^2}$ and modification of the intensity of the Delta dirac function in y direction. We note that it is possible to use the results of the first example with the above mapping but here the aim is to examine the capability of the method for solution of problems with orthotropic materials using square elements, as shown in Figure 3-a, for the cells. The numerical and exact solutions of the problem are shown in Figure 10. Here again 40 cells are used along each axis for

boundary conditions but 60 points are employed for integration. It can be seen again that the proposed method is capable of giving numerical solution to the problem.

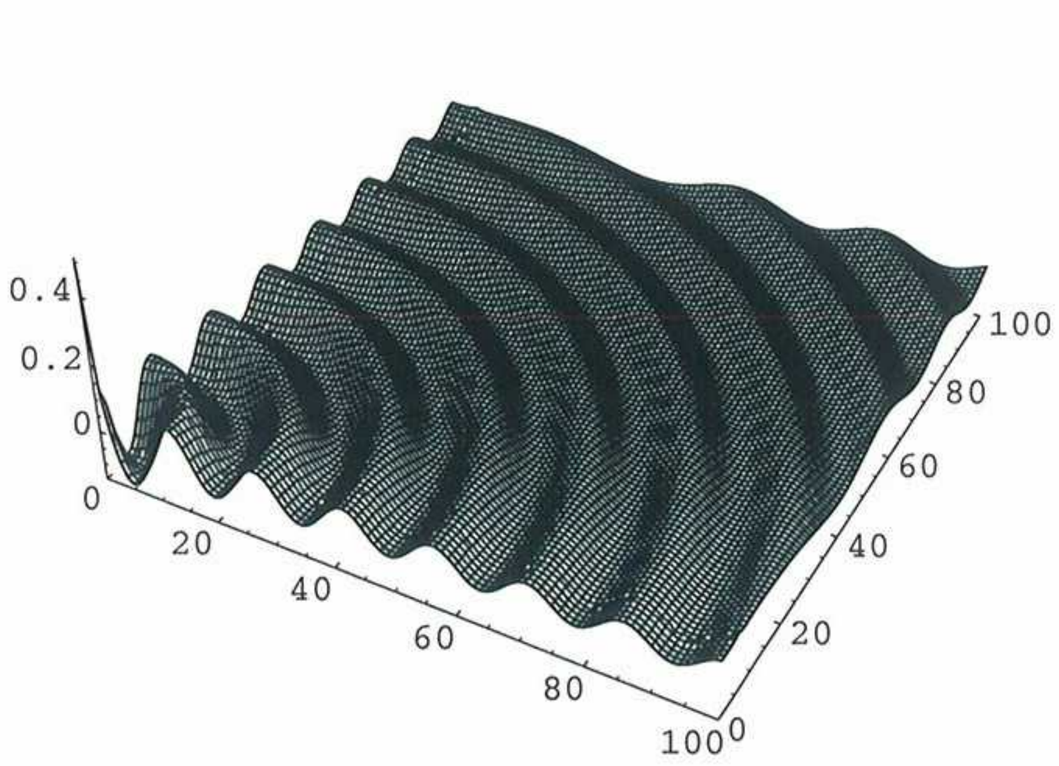

(a) FEM- $\Re(u)$

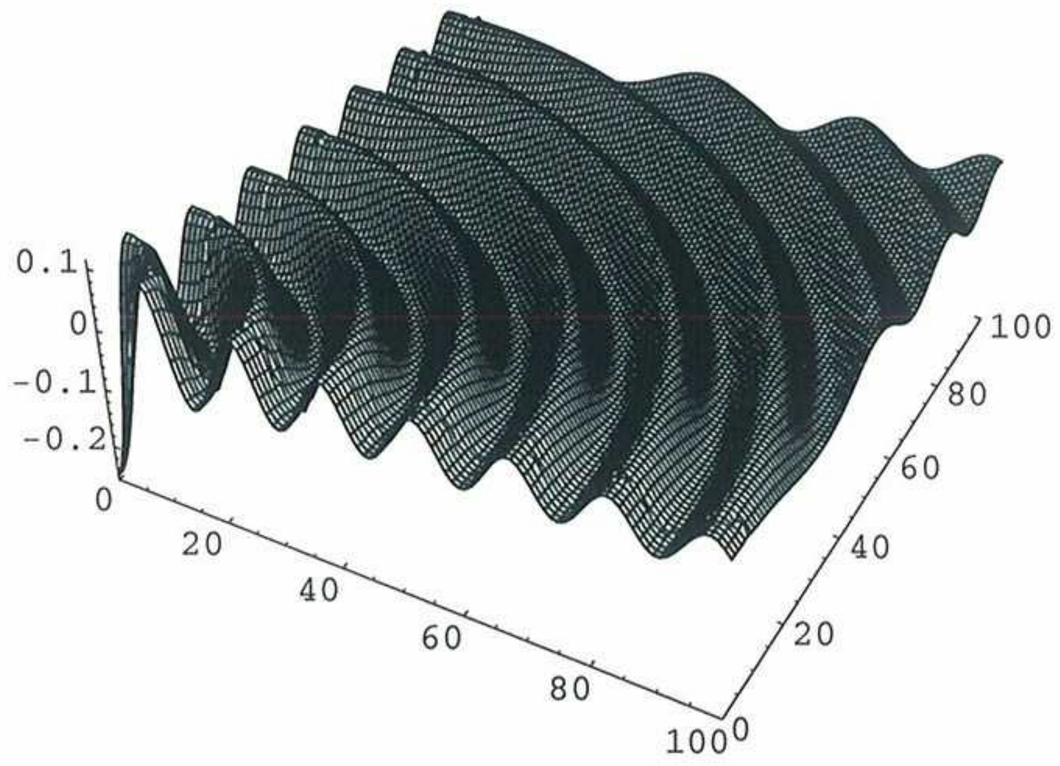

(b) FEM- $\Im(u)$

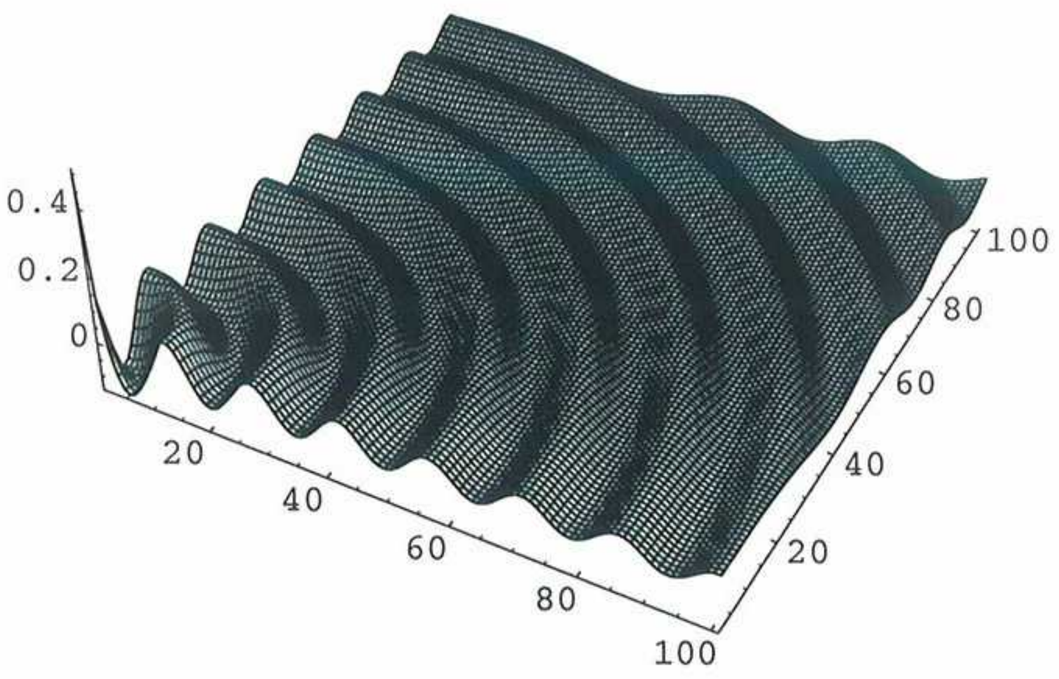

(c) Exact- $\Re(u)$

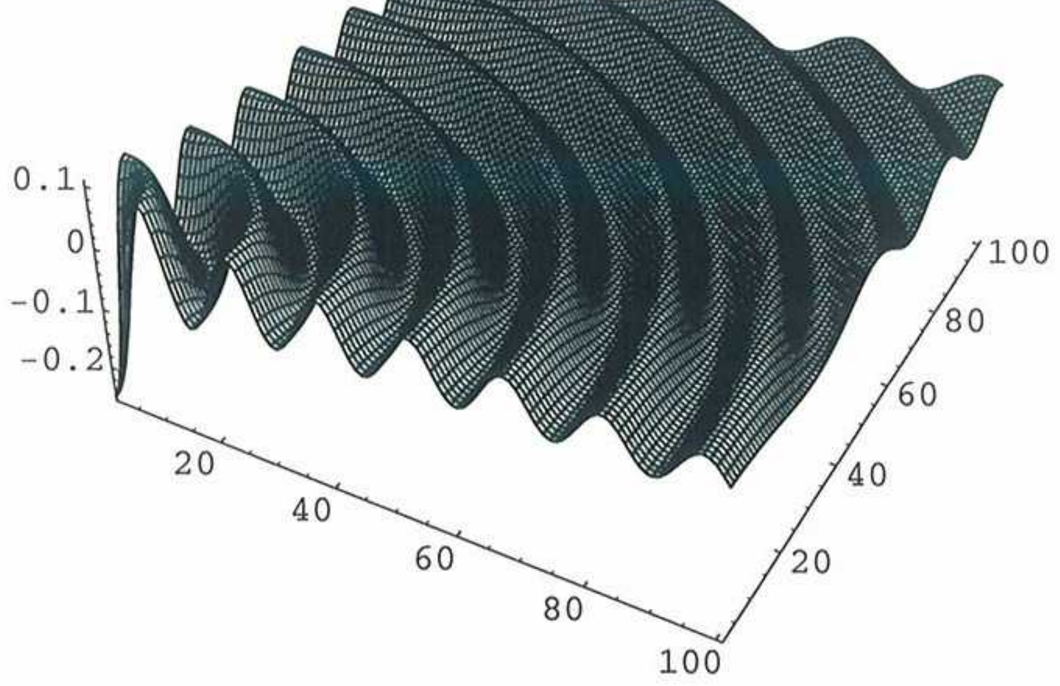

(d) Exact- $\Im(u)$

Figure 9. Variation of the real and imaginary parts of the solution of scalar wave problem shown over a domain of 100×100 cells. In numerical solution, 100 cells are used along each axis for satisfaction of the boundary conditions and also 100 points are used for integrations.

Example 3. As a benchmark problem for elastic wave category, we try to give numerical presentation of Green's function in a two dimensional infinite plane. Plane strain condition is assumed and unit harmonic point load is applied at origin of the coordinate system (x, y) in the direction of x. The corresponding differential equation is defined by Equations (20) and (21). The exact solutions for components of displacements, u and v, can be found in [27] as

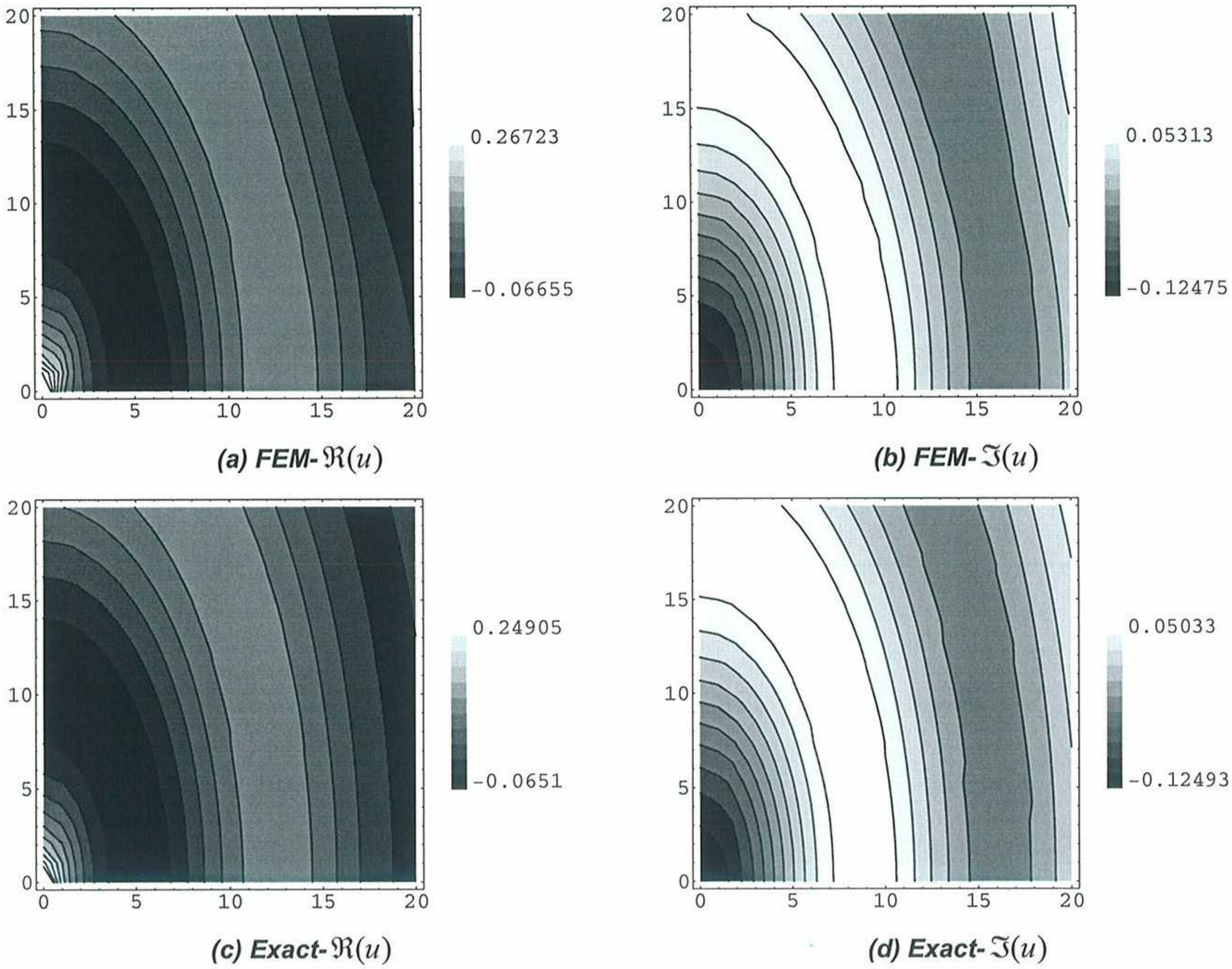

(a) FEM- $\Re(u)$ *(b) FEM-* $\Im(u)$

(c) Exact- $\Re(u)$ *(d) Exact-* $\Im(u)$

Figure 10. Contour plots of real and imaginary parts of the solution in scalar wave equation with $k_y = 4k_x$ ***. Forty cells are used along each axis for satisfaction of boundary conditions. The solutions are plotted over an area of*** 20×20 ***cells.***

$$u = \frac{1}{2\pi c_s^2}\left\{ K_0(\frac{i\omega r}{c_s}) - \frac{ic_s}{\omega r}\left(K_1(\frac{i\omega r}{c_s}) - \frac{c_s}{c_p} K_1(\frac{i\omega r}{c_p}) \right) - \left(K_2(\frac{i\omega r}{c_s}) - \frac{c_s^2}{c_p^2} K_2(\frac{i\omega r}{c_p}) \right)(\cos\theta)^2 \right\}$$

$$v = \frac{-\sin 2\theta}{4\pi c_s^2}\left(K_2(\frac{i\omega r}{c_s}) - \frac{c_s^2}{c_p^2} K_2(\frac{i\omega r}{c_p}) \right)$$

where K_n is the modified Bessel function of order n and of the second kind, ($,\theta$) represent polar coordinates of the point and c_s, c_p denote shear and pressure wave speeds, respectively, which are written in terms of shear and bulk modulus of the material

$$c_s = \sqrt{\frac{E}{2(1+\nu)\rho}} \qquad c_p = \sqrt{\frac{E}{3(1-2\nu)\rho}}$$

with ρ, E and ν being the density, elastic modulus and the Poisson's ratio of the material. In this example $\rho = 1$, $E = 1000$ and $\nu = 0.3$. Also ω is the frequency of the applied load which is chosen in this study so that $\omega^2 = 1000$.

For numerical solution the cell patterns shown in Figure 3-a-b-c are again used in this example. In order to model the problem in a quarter of the infinite plane, i.e. $x \geq 0$ and $y \geq 0$, the following symmetric and anti-symmetric conditions are used

$$v\big|_{x=0} = 0, \quad v\big|_{y=0} = 0, \quad \tau_{xy}\big|_{y=0} = 0 \text{ and } \sigma_x\big|_{x=0} = 0$$

where σ and τ denote normal and shear stresses. Here again 40 boundary cells are considered for satisfying the boundary conditions along x and y. Also the number of integration points on Gaussian plane is 40 for radial and angular directions separately. Figures 11 to 14 depict variations of the two displacement components over an area of 20×20 cells. The figures clearly show that the proposed method is capable of producing finite element solution.

Comparison with the exact values shows that solution with linear quadrilateral elements exhibits dispersion effect along $y = 0$ especially for u displacement. This can be understood by measuring the spacing between the contour lines along $y = 0$. Considering the direction of the applied unit load and the boundary conditions, gradients of u displacement along $y = 0$ represent deformation due to longitudinal component of the waves. For the same displacement, however, variation along $x = 0$ seems to be similar to the exact solution. Deformations associated with this latter case represent shear waves. The overall conclusion is that linear quadrilateral elements perform better in shear wave deformation rather than longitudinal waves especially along the edges. This coincides with observations and analytical studies made by Cherukuri in [19].

For regular pattern of triangular elements, Figures 11-c-d to 14-c-d show that the directional behavior is more pronounced than that of the case for solution of scalar wave problem. Figure 14-d clearly demonstrates the skewness of the deformation due to the directional behavior of the cell. Figures 11-e and 11-e-f and 14-e-f depict the results obtained from use of Criss-Cross pattern of cells. As expected, the directional behavior is reduced and similar results to those obtained from linear quadrilateral elements are achieved.

In Figures 15 and 16 the distribution of the numerical solution is shown over an area of 100×100 cells. Hundred of integration points are used to satisfy boundary conditions on 100 cells along the axes. As the first example, here again, procedure of Appendix A with machine precision has been employed. Better presentation of dispersion is seen along $y = 0$ when real and imaginary parts of u displacement, Figure 15-a and 15-b, are compared with the exact ones in Figures 15-c and 16-d.

For convergence study we present Figure 17 in which norms of the solutions with different number of integration points are given. Similar to the first example, 40 cells are used along each axis for satisfaction of the boundary conditions and the norms are calculated over an area of 20×20 cells. The difference between norms for above 40 integration points is less than 0.05% for Criss-Cross pattern and less than 0.09% for linear quadrilateral elements which are in the same order and show very good convergence. Again an important observation is that the minimum number of integration points is within the order of the number of cells used for satisfaction of boundary conditions along the x and y axes.

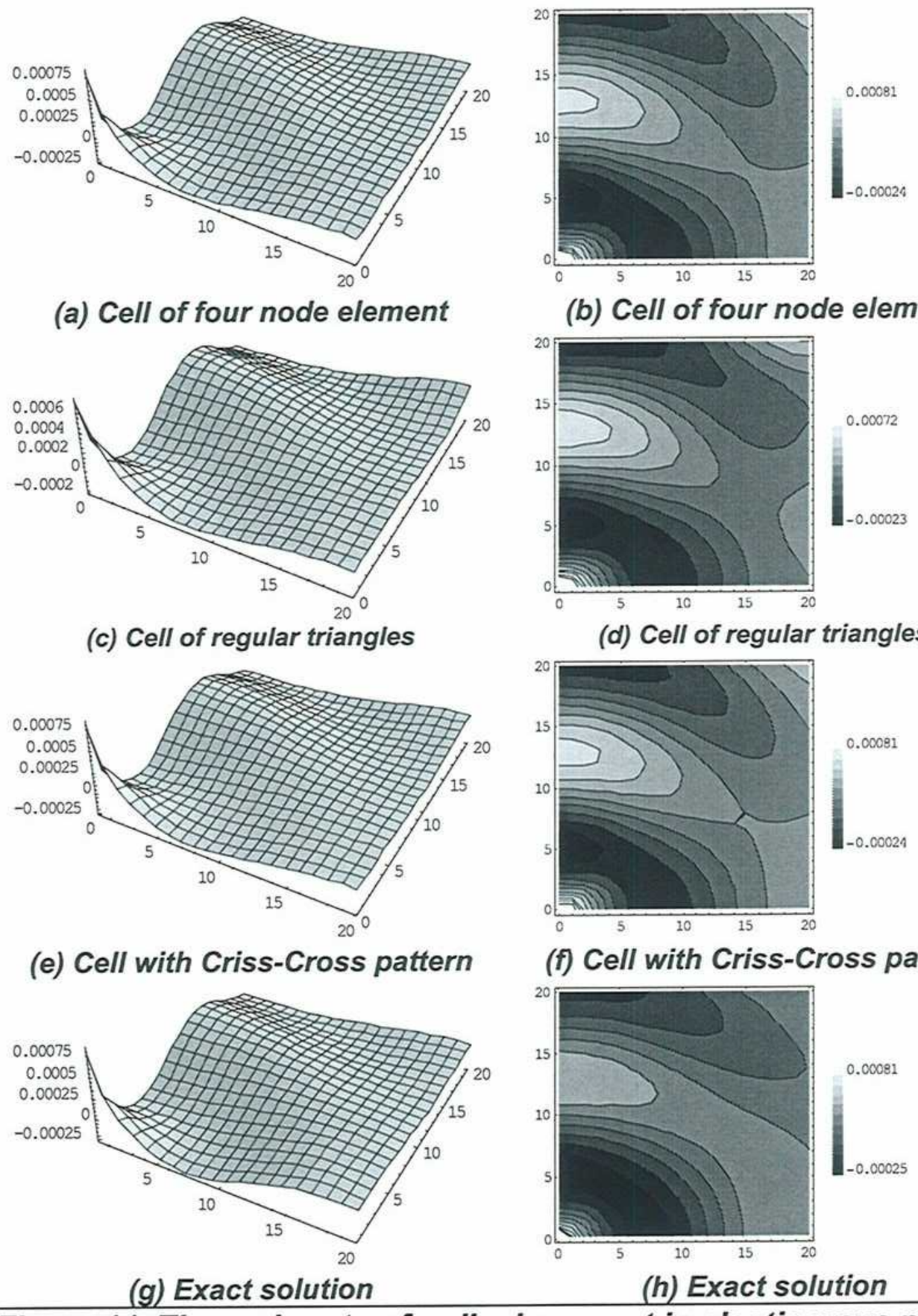

Figure 11. The real parts of u displacement in elastic wave problem. The numbers on x and y axes represent the number of cells used. Forty cells are used along each axis for satisfaction of the boundary conditions. The solutions are plotted over an area of 20 × 20 cells.

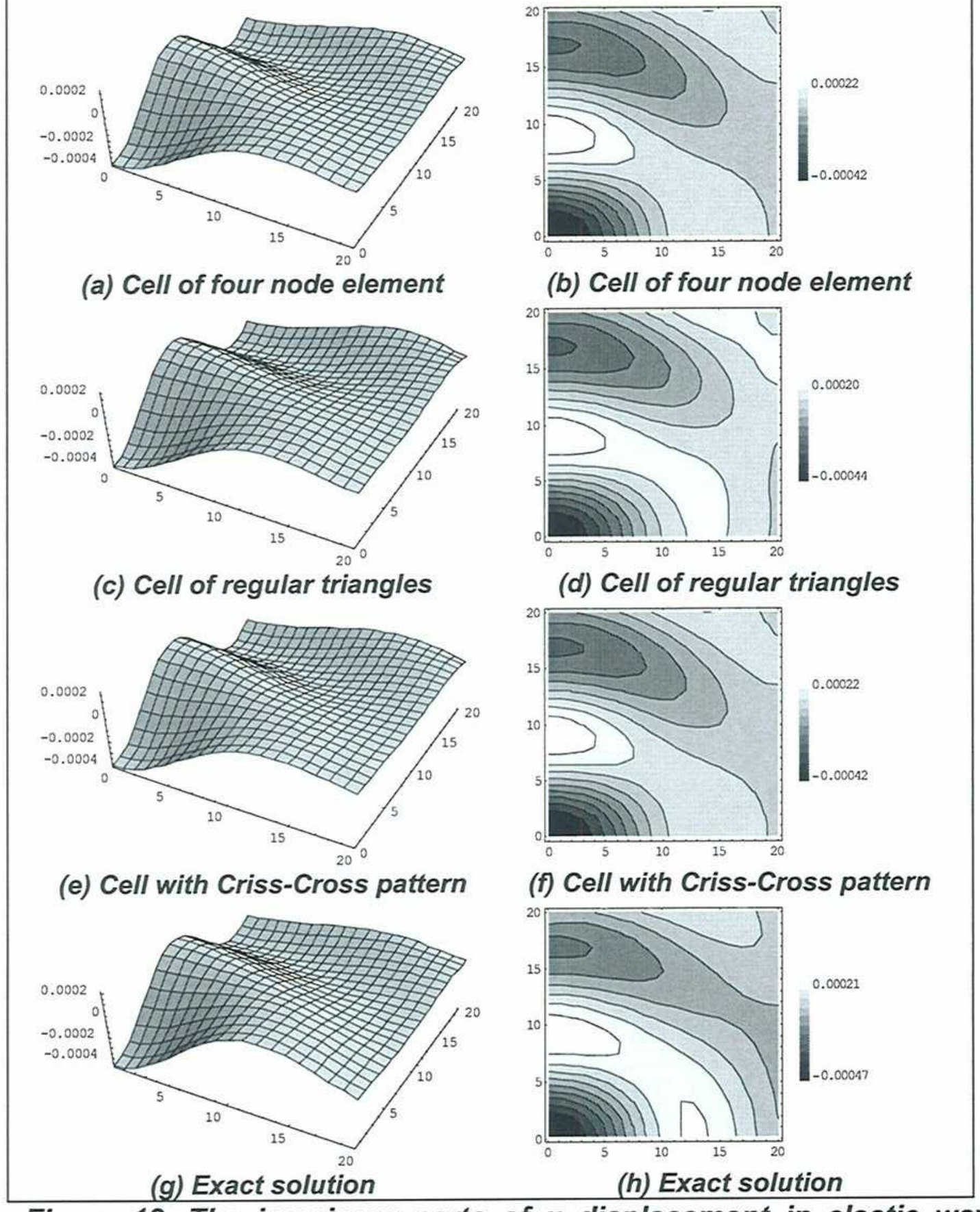

Figure 12. The imaginary parts of u displacement in elastic wave problem. The numbers on x and y axes represent the number of cells used. Forty cells are used along each axis for satisfaction of the boundary conditions. The solutions are plotted over an area of 20 × 20 cells.

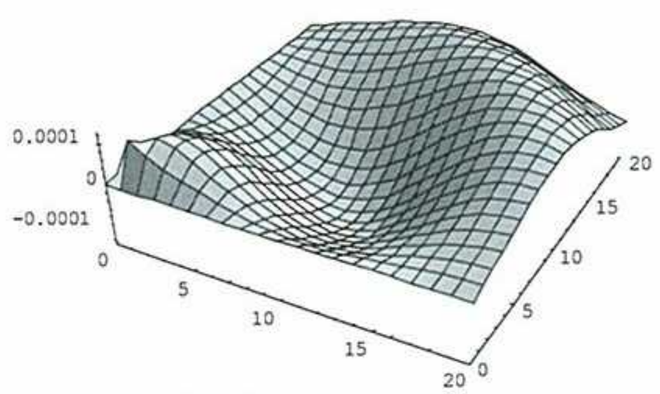

(a) Cell of four node element

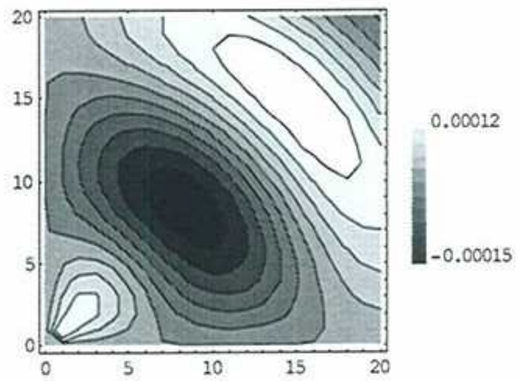

(b) Cell of four node element

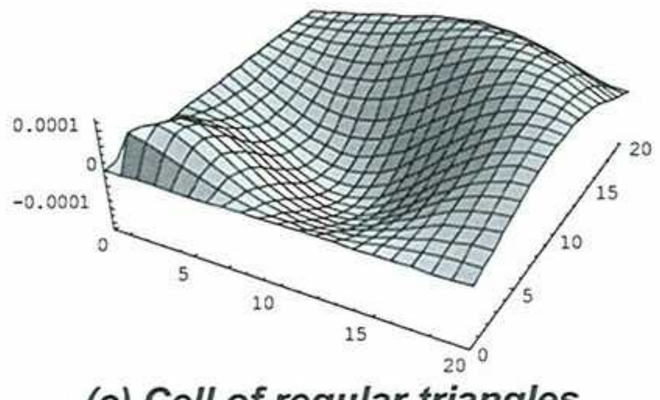

(c) Cell of regular triangles

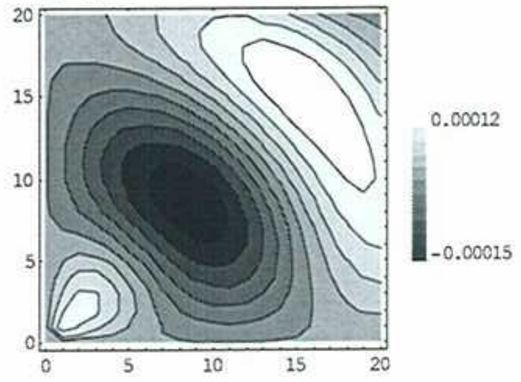

(d) Cell of regular triangles

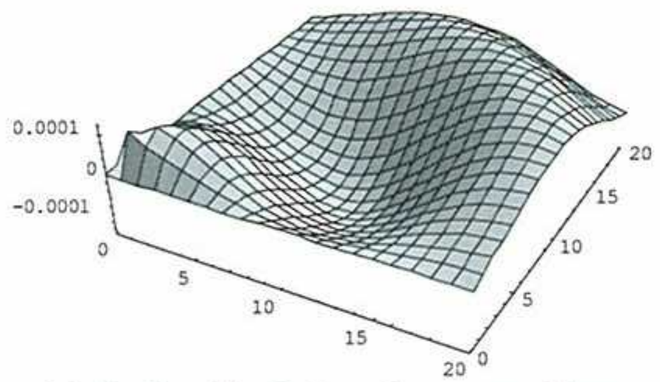

(e) Cell with Criss-Cross pattern

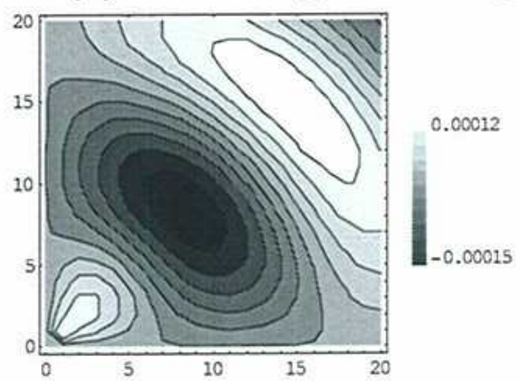

(f) Cell with Criss-Cross pattern

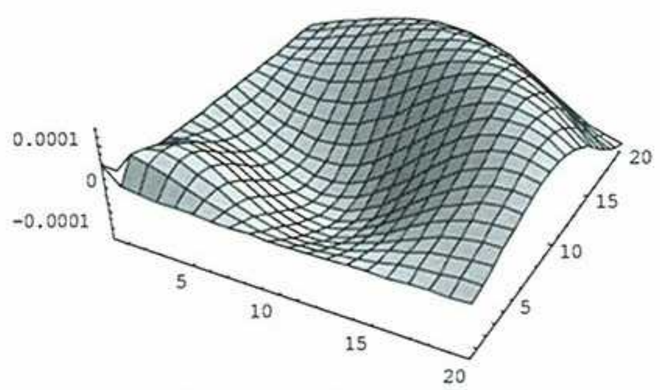

(g) Exact solution

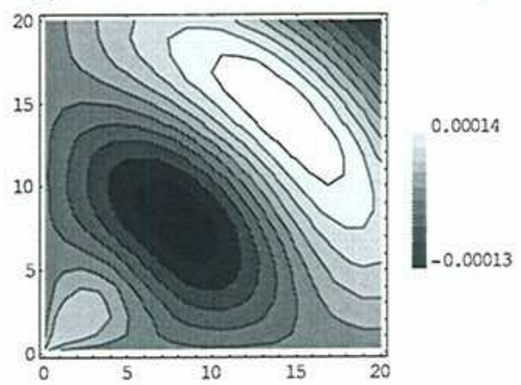

(h) Exact solution

Figure 13. The real parts of v displacement in elastic wave problem. The numbers on x and y axes represent the number of cells used. Forty cells are used along each axis for satisfaction of the boundary conditions. The solutions are plotted over an area of 20×20 cells.

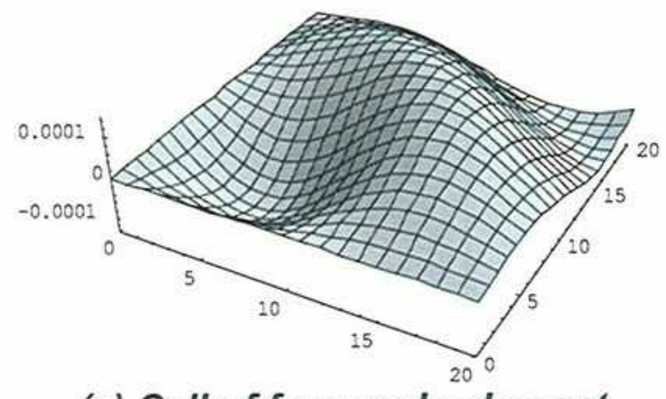

(a) Cell of four node element

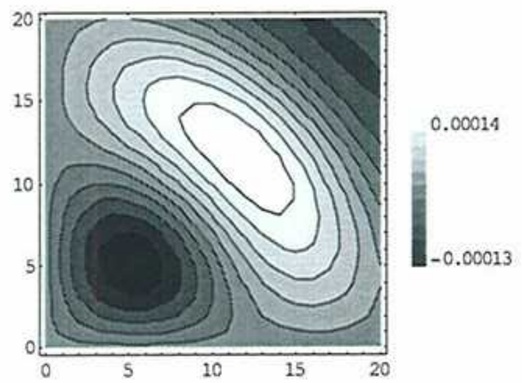

(b) Cell of four node element

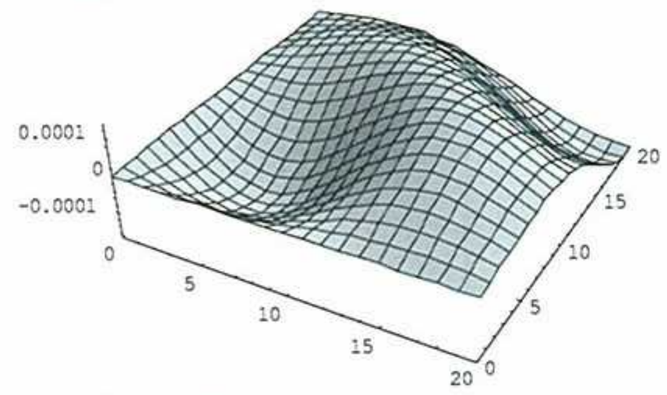

(c) Cell of regular triangles

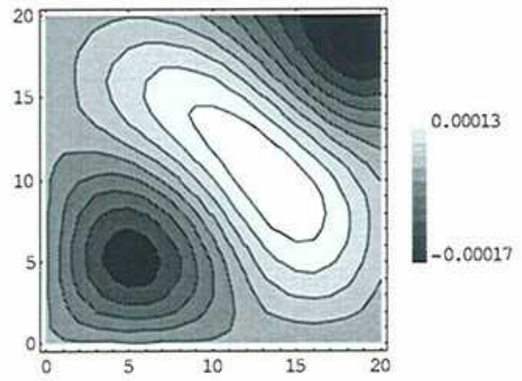

(d) Cell of regular triangles

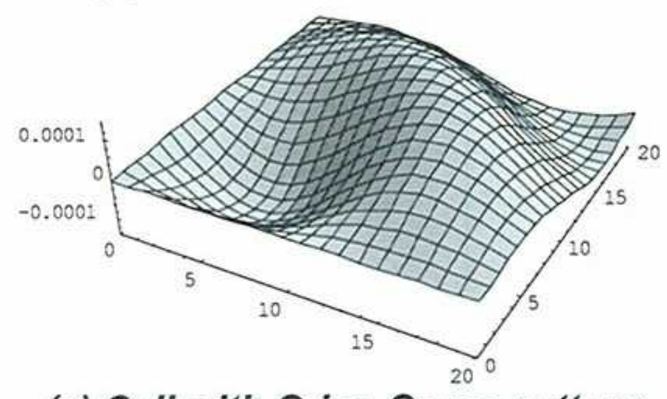

(e) Cell with Criss-Cross pattern

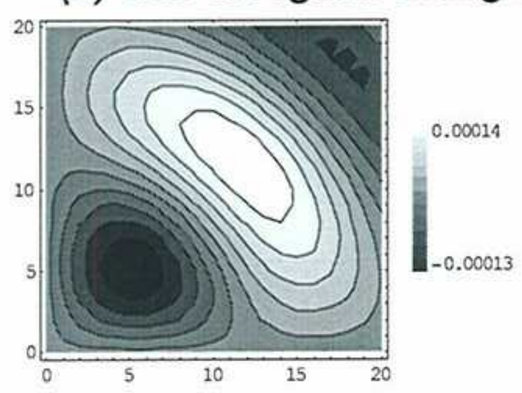

(f) Cell with Criss-Cross pattern

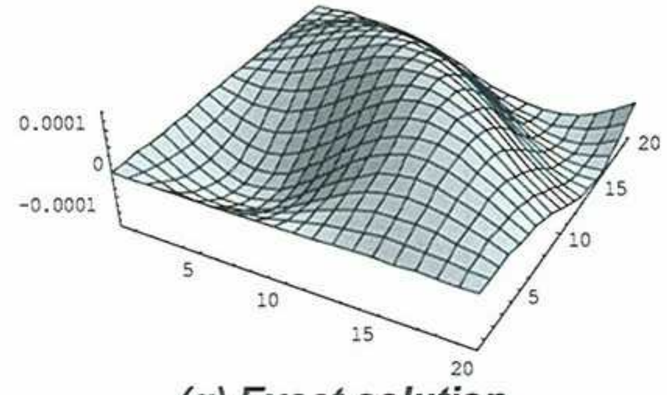

(g) Exact solution

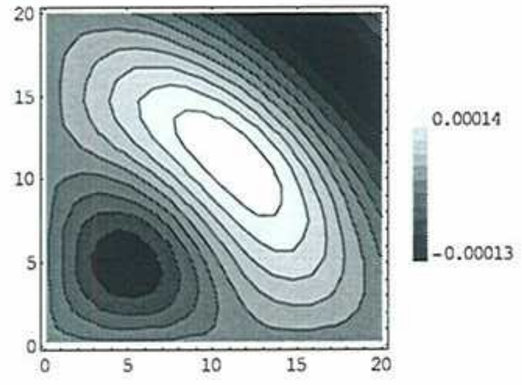

(h) Exact solution

Figure 14. The imaginary parts of v displacement in elastic wave problem. The numbers on x and y axes represent the number of cells used. Forty cells are used along each axis for satisfaction of the boundary conditions. The solutions are plotted over an area of 20×20 cells.

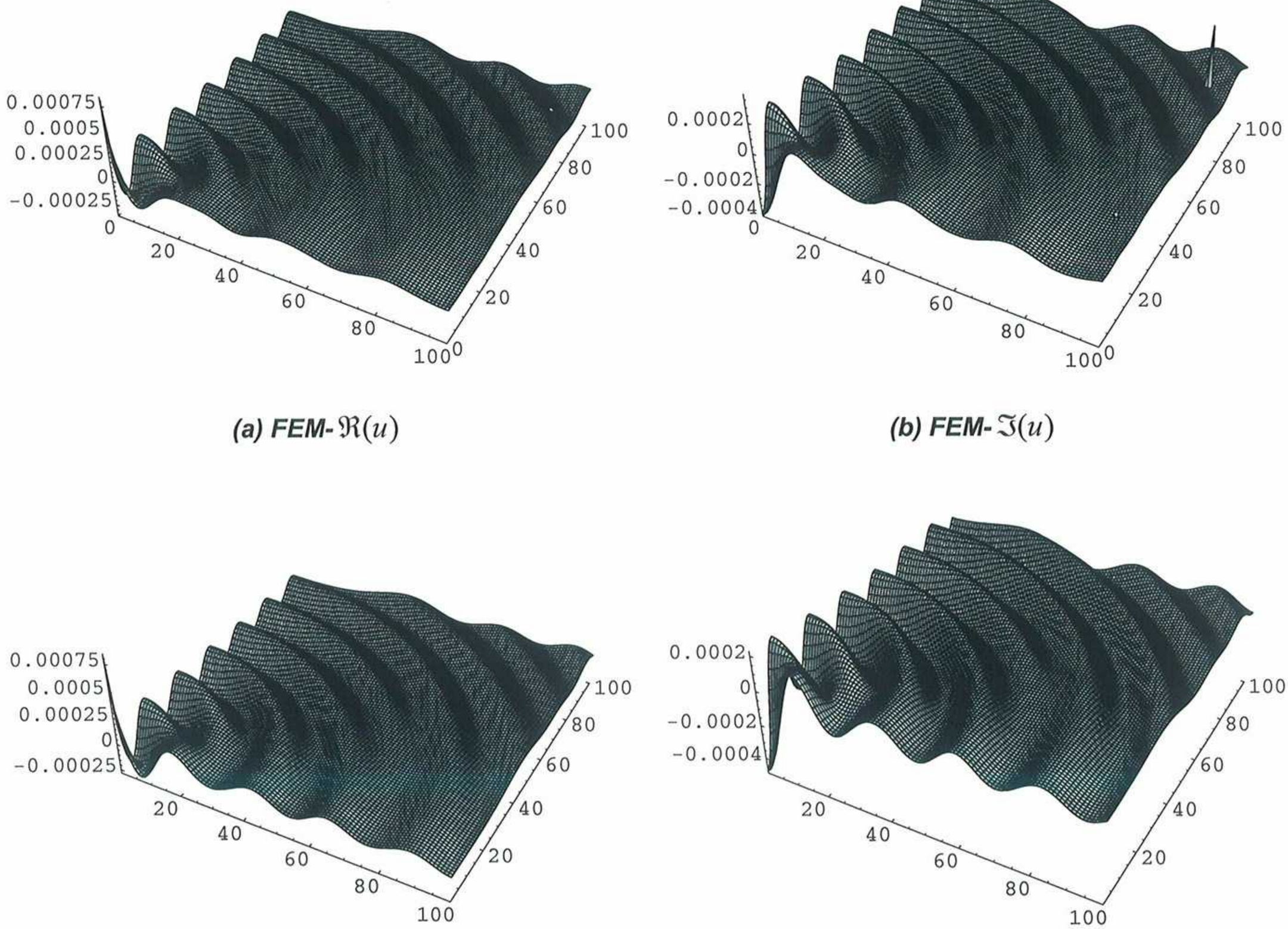

(a) FEM- $\Re(u)$ *(b) FEM-* $\Im(u)$

(c) Exact- $\Re(u)$ *(d) FEM-* $\Im(u)$

Figure 15. Variation of the real and imaginary parts of u displacement in elastic wave problem shown over a domain of 100×100 cell of single quadrilaterals. In numerical solution, 100 cells are used along each axis for satisfaction of the boundary conditions and also 100 points are used for integrations.

Figure 18 demonstrates convergence of the solution with respect to the number of cells used along each axis. For evaluation of the norms an area of 20×20 cells is used. The figure clearly shows the method proposed in this report is convergent with respect to the number of cells for boundary conditions.

5. CONCLUSIONS

In this report we have presented a numerical solution method to wave problems with constant coefficient differential equations. We have aimed at presenting Green's functions in frequency domain, as the representatives of wave problems, in a numerical manner. It has been shown that a proportionality property exists in the solution since the general solution of the governing differential equation can analytically be written as a summation of some exponential functions. Similar proportionality effect has been assumed in the numerical solution when the grid is of repeatable patterns (named as "cells"). It has been shown that such an effect also leads to sequential similarity in

the rows of coefficient matrix. Application of the proportionality in columns of a generic series of rows, results in an eigen value like problem through which a characteristic equation, consisting of the proportionality values along main axes, is defined.

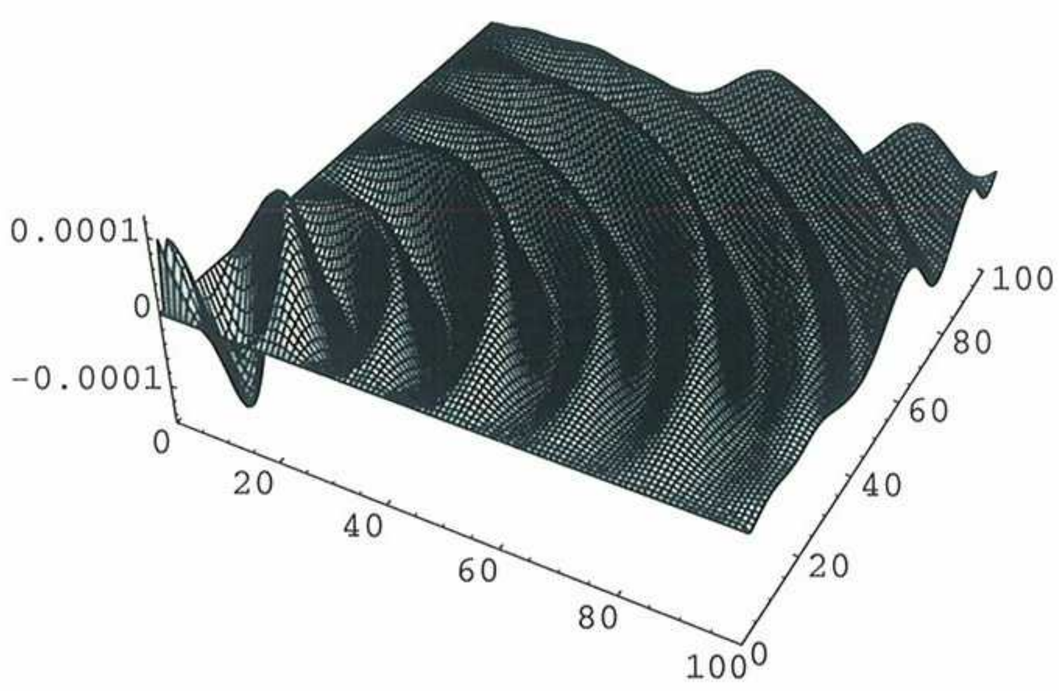

(a) FEM- $\Re(v)$

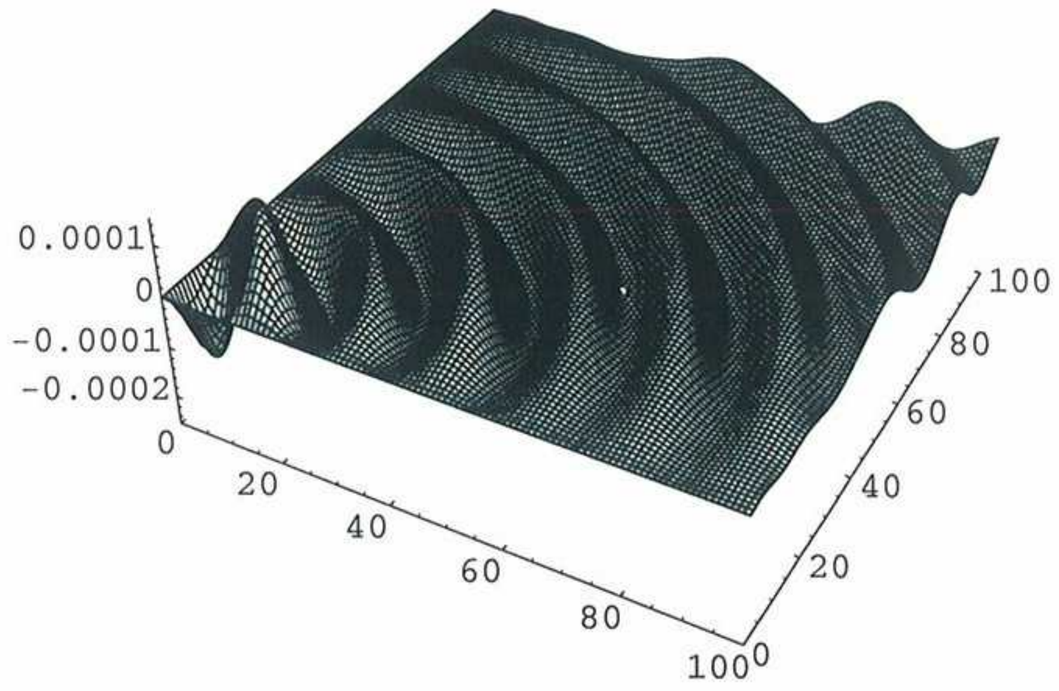

(b) FEM- $\Im(v)$

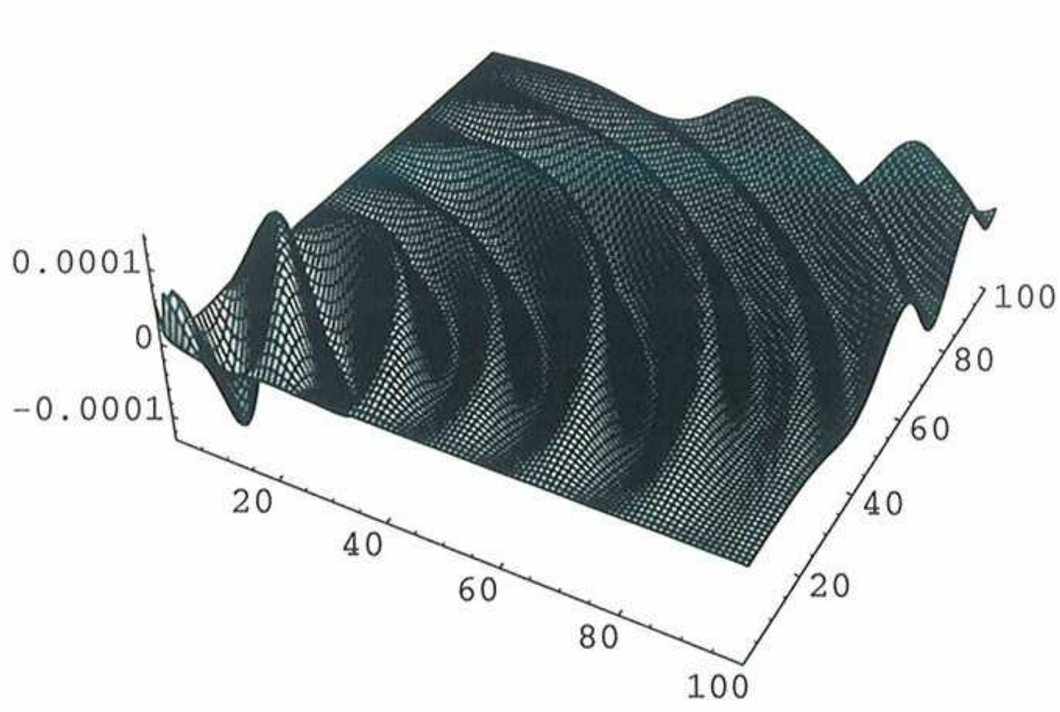

(c) Exact- $\Re(v)$

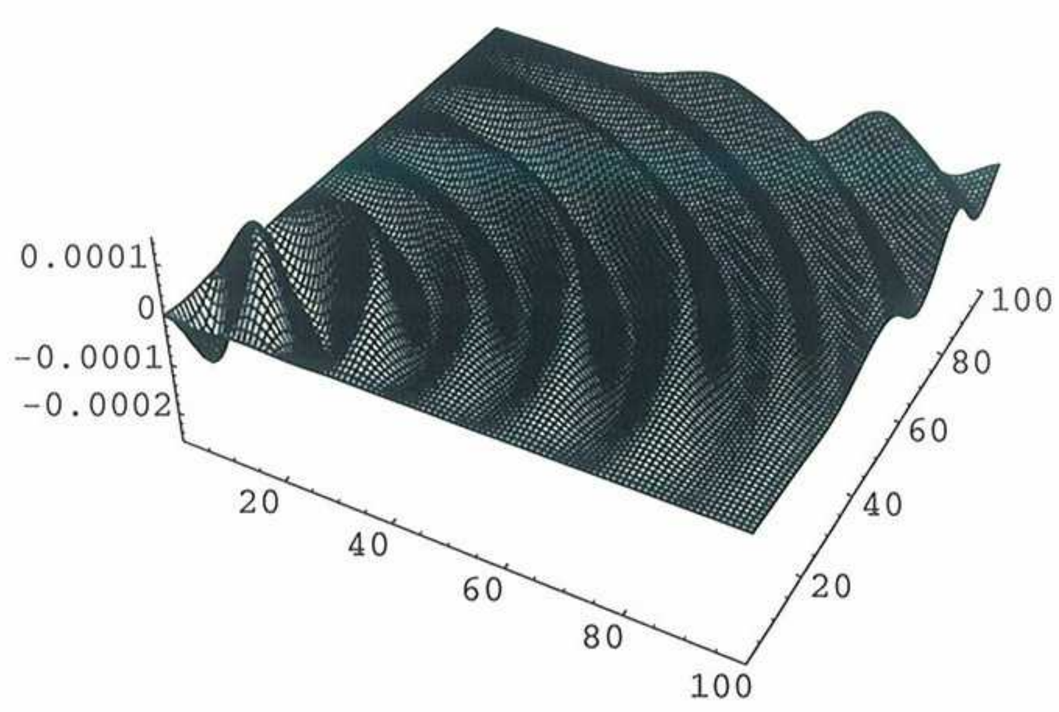

(d) Exact- $\Im(v)$

Figure 16. Variation of the real and imaginary parts of v displacement in elastic wave problem shown over a domain of 100×100 cell of single quadrilaterals. In numerical solution, 100 cells are used along each axis for satisfaction of the boundary conditions and also 100 points are used for integrations.

It has been shown that the numerical solution may be obtained in a spectral form through evaluation of the roots of the characteristic equation and associated null space bases. Both decay and radiation conditions are satisfied by defining a feasible domain for roots of the characteristic equation in Gaussian plane. A compatible transformation technique has also been introduced for satisfaction of the boundary conditions. Neumann, Dirichlet and mixed boundary conditions are considered for the solution.

Finite element method has been employed as the numerical solution technique. Some benchmark problems, in scalar and elastic wave categories, have been solved and the results of the numerical

Green's functions have been compared to those from analytical solutions. Several patterns for cells are used for numerical solution. Convergence of the results, in terms of the number of cells along the main axes and integration points in Gaussian plane, has also been addressed. The studies show that the method leads to convergent results.

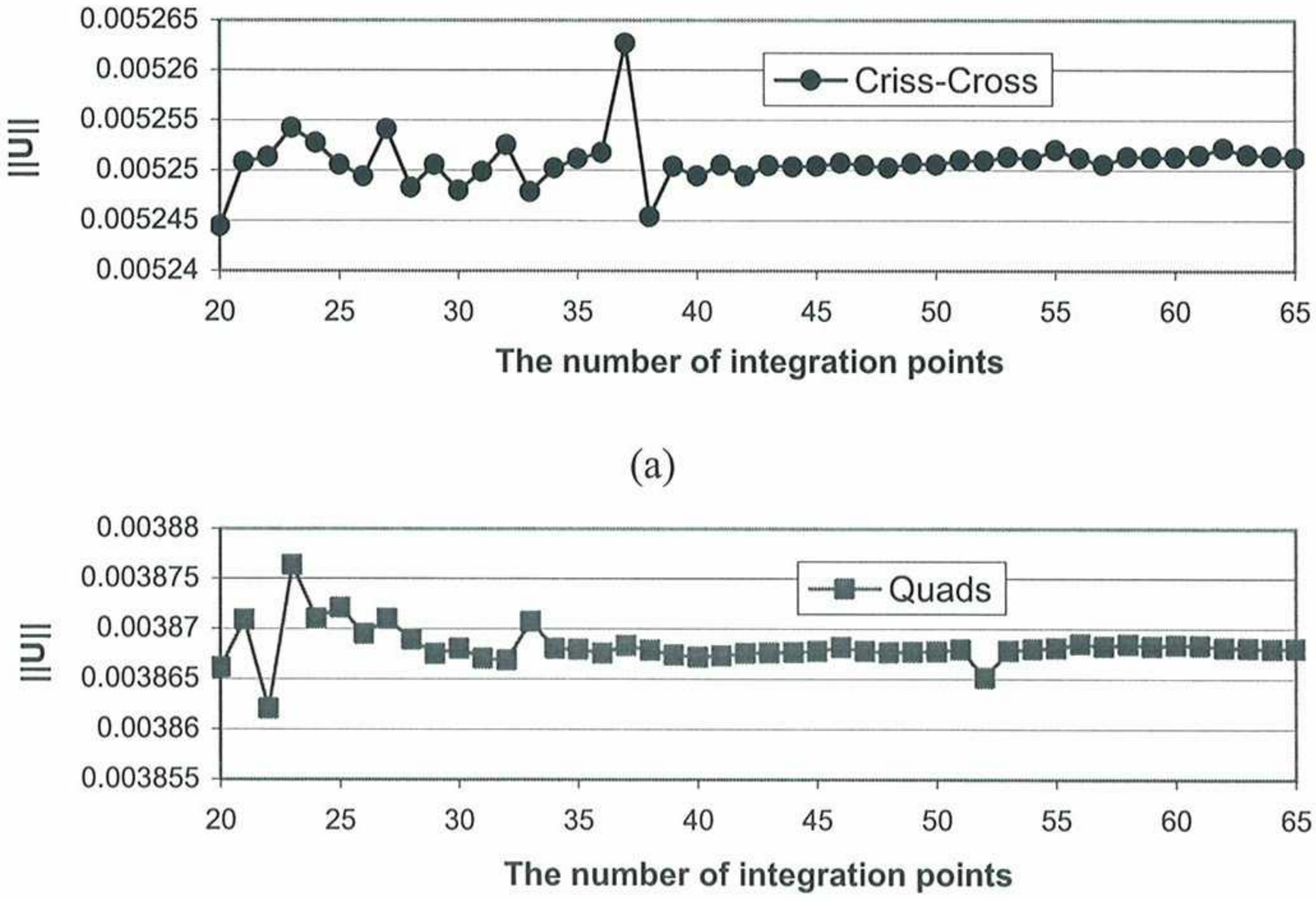

Figure 17. Variation of L_2 norms of the solution, for elastic wave problem, versus the number of integration points used for different patterns of cells. The norms are calculated over an area of 20×20 cells and 40 cells are used along each axis for satisfaction of the boundary conditions.

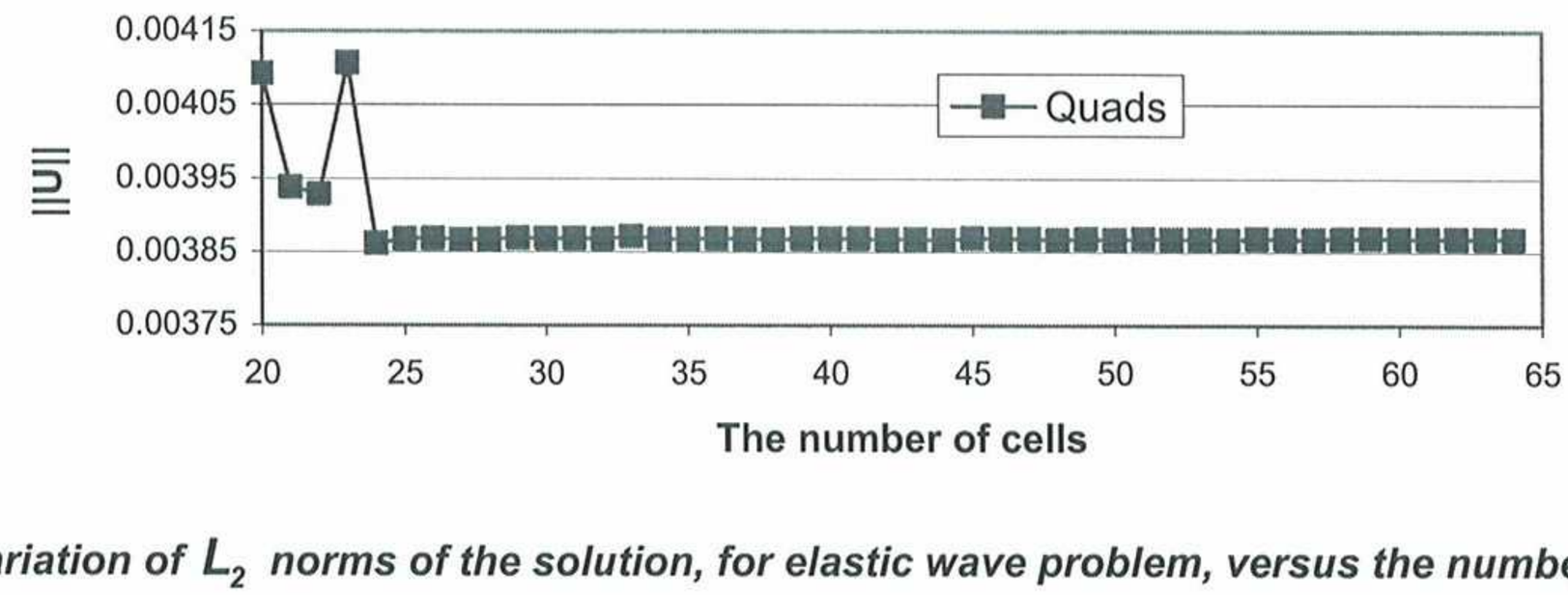

Figure 18. Variation of L_2 norms of the solution, for elastic wave problem, versus the number of cells used for satisfaction of boundary conditions. The norms are calculated over an area of 20×20 cells and 40 points are used for integrations

Appendix A

When machine precision is used in computations, one may confront with some ill-conditioned matrices. In this part we give a remedy for reducing such an effect.

In order to study possibilities of avoiding inversion of the matrix given in (55), one may rewrite Equation (62) as

$$\mathbf{G}\mathbf{R}\bar{\mathbf{u}}_B = \mathbf{f}_t \qquad \mathbf{G} = \mathbf{K}_{bnd}\left(\sum \mathbf{v'}^{n}_{k(\mu_n)}\left(\mathbf{v}^{n}_{k(\mu_n)}\right)^T\right) \tag{A-1}$$

and thus

$$\mathbf{R}\bar{\mathbf{u}}_B = \mathbf{G}^{-1}\mathbf{f}_t \tag{A-2}$$

or

$$\bar{\mathbf{u}}_B = \mathbf{H}\mathbf{f}_t \qquad \mathbf{H} = \mathbf{R}^{-1}\mathbf{G}^{-1} = \left[\sum \mathbf{v}^{n}_{k(\mu_n)}\left(\mathbf{v}^{n}_{k(\mu_n)}\right)^T\right]\left[\mathbf{K}_{bnd}\sum \mathbf{v'}^{n}_{k(\mu_n)}\left(\mathbf{v}^{n}_{k(\mu_n)}\right)^T\right]^{-1} \tag{A-3}$$

It may be seen that the inverse of the last bracket is still needed. Our experience also shows that the matrix in the second bracket is less sensitive to round off errors than the one in the first bracket.

For problems with pure Neumann boundary conditions relation (A-2) may directly be used for evaluation of the finite element solution through (57) as

$$\bar{\mathbf{u}} = \left(\sum \mathbf{w}^{n}_{k(\mu_n)}\left(\mathbf{v}^{n}_{k(\mu_n)}\right)^T\right)\mathbf{G}^{-1}\mathbf{f} \tag{A-4}$$

For mixed Dirichlet-Neumann boundary conditions, first equation in (A-3) is written in partitioned form

$$\begin{Bmatrix}\bar{\mathbf{u}}_{B1}\\ \bar{\mathbf{u}}_{B0}\end{Bmatrix} = \begin{bmatrix}\mathbf{H}_{11} & \mathbf{H}_{12}\\ \mathbf{H}_{21} & \mathbf{H}_{22}\end{bmatrix}\begin{Bmatrix}\mathbf{f}_{t0}\\ \mathbf{f}_{t1}\end{Bmatrix} \tag{A-5}$$

In which vectors $\bar{\mathbf{u}}_{B0}$ and $\mathbf{f}_{t0}$ are the prescribed displacement and nodal forces. In order to use (A-4), vector of unknown nodal forces $\mathbf{f}_{t1}$ must be determined. From the second row of the equations in (A-5) one can write

$$\mathbf{f}_{t1} = \mathbf{H}_{22}^{-1}(\bar{\mathbf{u}}_{B0} - \mathbf{H}_{21}\mathbf{f}_{t0}) \tag{A-6}$$

The rest of procedure is to arrange the nodal forces as $\mathbf{f}_t = \begin{bmatrix}\mathbf{f}_{t0}^T & \mathbf{f}_{t1}^T\end{bmatrix}^T$ and substitute it in (A-4). It can be seen that in the mixed form of boundary condition we just need the inverse of matrix $\mathbf{H}_{22}$ which is a part of the matrix defined in (A-3). Experience shows that results from (A-4) and (A-5) are more accurate than those from direct use of equations (57) and (62) which require evaluation of $\mathbf{R}$ as (55).

However, when the boundary conditions are of pure Dirichlet form there is no escaping way from evaluation of $\mathbf{R}$ if (63) is used. Nevertheless, one can use the set of equations given in (65) to (68). For this, by virtue of (65) and (66), one may write

$$\bar{\mathbf{u}}' = \left(\sum \mathbf{v}^{n}_{k(\mu_n)} \left(\mathbf{v}'^{n}_{k(\mu_n)} \right)^T \right) \mathbf{K}^T_{bnd} \mathbf{R}' \mathbf{f}_t \qquad \text{(A-7)}$$

or

$$\bar{\mathbf{u}}' = \mathbf{G}^T \mathbf{R}' \mathbf{f}_t \qquad \text{(A-8)}$$

with $\mathbf{G}$ defined as (A-1). Then by use of (68) and noting that

$$\mathbf{G}^{-T} \bar{\mathbf{u}}' = \mathbf{R}' \mathbf{f}_t \qquad \text{(A-9)}$$

the finite element solution for the whole domain can be written as

$$\bar{\mathbf{u}} = \left(\sum \mathbf{w}^{n}_{k(\mu_n)} \left(\mathbf{v}'^{n}_{k(\mu_n)} \right)^T \right) \mathbf{K}^T_{bnd} \mathbf{G}^{-T} \bar{\mathbf{u}}' \qquad \text{(A-10)}$$

Note that Equations (65) and (66), in Remark 5, were originally proposed for pure Neumann boundary condition but here we used them for pure Dirichlet.

It is therefore seen that except for problems with pure Neumann or pure Dirichlet boundary conditions, at least inversion of a part of the matrix defined in (55) is needed and thus round off error may still encounter the computations when machine precision is used. As an effective way for further reduction of such an effect, the decimal numbers in components of vectors $\mathbf{v}'^{n}_{k(\mu_n)}$, $\mathbf{v}^{n}_{k(\mu_n)}$ and $\mathbf{w}^{n}_{k(\mu_n)}$ may be truncated. By doing so, depending on the truncated decimals, the effects of highly decaying modes are ignored in far field solution. In this report decimal numbers are truncated up to 10^{-3} for problems solved in examples 1 and 3.

Appendix B

In this part we give some expressions for the $\mathbf{Q}$ matrices, resulted from substitution of relations (32) in (30) and defined as (34).

a) Scalar wave problems : For this case, when patterns like Figures 3-a and 3-c are used, $\mathbf{Q}$ is a scalar. Denote the cell lengths in x and y directions as a and b respectively, and let k_x, k_y and k_{xy} be coefficients in modulus of material matrix.

a-1) For linear quadrilateral elements (Fig 3-a):

Defining following factors

$\alpha = \rho\omega^2$

$$f_1 = b^2 k_x + 3abk_{xy} + a^2 k_y \qquad f_2 = -6k_x + a^2\alpha \qquad f_3 = 3k_x + a^2\alpha$$

$$g_1 = 18abk_{xy} - 6a^2k_y + b^2f_2 \quad g_2 = 3a^2k_y + b^2f_2 \quad g_3 = -6a^2k_y + b^2f_3 \quad g_4 = -6f_1 + a^2b^2\alpha \quad g_5 = 3a^2k_y + b^2f_3$$

(B-1)

then **Q** is evaluated as

$$Q(\mu_1,\mu_2) = \frac{1}{36ab\mu_1\mu_2}(g_4 + 4g_2\mu_2 + g_1\mu_2^2 + 4\mu_1(g_3 + 4g_5\mu_2 + g_3\mu_2^2) + \mu_1^2(g_1 + \mu_2(4(3g_2 + g_4\mu_2)))$$

(B-2)

The characteristic equation is obtained when the determinant of **Q** is set to zero, i.e. in this case $Q(\mu_1,\mu_2) = 0$.

a-2) For Criss-Cross pattern

Defining following factors

$$f_1 = 12a^2k_y + 12b^2k_x + a^2b^2\alpha \qquad f_2 = 12a^2k_y + 12b^2k_x - a^2b^2\alpha \qquad f_3 = b^4(12k_x - a^2\alpha)(36k_x + a^2\alpha)$$
$$f_4 = a^2b^2(8k_{xy}^2 - 4k_xk_y + a^2k_y\alpha) \qquad f_5 = a^2b^2(24k_{xy}^2 - 12k_xk_y + a^2k_y\alpha) \qquad f_6 = b^4(144k_x^2 + 72a^2k_x\alpha + a^4\alpha^2)$$
$$f_7 = a^2b^2(-24k_{xy}^2 + 36k_xk_y + 7a^2k_y\alpha) \qquad f_8 = a^4(432k_x^2 + 168a^2k_x\alpha + 7a^4\alpha^2)$$

$$g_1 = (24abk_{xy} + f_2)^2 \qquad g_2 = (24abk_{xy} - f_2)^2 \qquad g_3 = -144a^4k_y^2 + f_3 - 72f_4$$
$$g_4 = -432a^4k_y^2 + 24f_5 + f_6 \qquad g_5 = 864a^4k_y^2 + 48f_7 + 2f_8$$

(B-3)

then **Q** is evaluated as

$$Q(\mu_1,\mu_2) = -\frac{1}{96abf_1\mu_1\mu_2}(g_1 + 2g_3\mu_2 + g_2\mu_2^2 + \mu_1^2(g_2 + \mu_2(2g_3 + g_1\mu_2)) - 2\mu_1(g_4 + \mu_2(g_5 + g_4\mu_2)))$$

(B-4)

b) Elastic wave problems : For this case, when patterns like Figures 3-a and 3-c are used, **Q** is a 2×2 matrix. i.e.

$$\mathbf{Q} = \begin{bmatrix} Q_{11} & Q_{12} \\ Q_{21} & Q_{22} \end{bmatrix}$$

(B-5)

Here again the cell lengths along x and y axes are denoted as a and b respectively. The material elastic modulus and Poisson's ratio are considered to be as E and ν.

b-1) For linear quadrilateral elements:

Defining following factors

$$\alpha = \rho\omega^2$$
$$F_1 = 1 - 2\nu \qquad F_2 = -1 + \nu \qquad F_3 = 1 + \nu$$

$$G_1 = a^2F_1 \quad G_2 = b^2F_1 \quad G_3 = a^2F_2 \quad G_4 = b^2F_2 \quad G_5 = a^2F_3 \quad G_6 = b^2F_3$$
$$H_1 = G_1(-3E + G_6\alpha) \quad H_2 = G_1(6E + 4G_6\alpha) \quad H_3 = G_2(-3E + G_5\alpha) \quad H_4 = G_2(3E + 2G_5\alpha)$$
$$I_1 = 6G_4E + H_1 \qquad I_2 = -3G_4E + H_1 \qquad I_3 = 6G_3E + H_3 \qquad I_4 = 12G_3E + H_4 \qquad I_5 = 24G_4E + H_2$$
$$I_6 = -12G_3E + 4H_3 \qquad I_7 = -12G_4E + H_2 \qquad I_8 = -6G_3E + H_4$$

(B-6)

then one obtains following expressions for elements of **Q**

$$Q_{11} = \frac{1}{36abF_1F_3\mu_1\mu_2}(I_1 + \mu_2(I_5 + I_1\mu_2) + 4\mu_1(I_1 + \mu_2(I_7 + I_1\mu_2)) + \mu_1^2(I_1 + \mu_2(I_5 + I_1\mu_2)))$$

$$Q_{12} = Q_{21} = -\frac{E(-1+\mu_1^2)(-1+\mu_2^2)}{8F_1F_3\mu_1\mu_2}$$

$$Q_{22} = \frac{1}{36abF_1F_3\mu_1\mu_2}(I_3 + \mu_2(I_6 + I_3\mu_2) + \mu_1^2(I_3 + \mu_2(I_6 + I_3\mu_2)) + 2\mu_1(I_4 + \mu_2(4I_8 + I_4\mu_2))) \qquad \text{(B-7)}$$

Here again the characteristic equation is obtained when the determinant of **Q** is set to zero, i.e. in this case $|\mathbf{Q}(\mu_1, \mu_2)| = 0$. The associated null space consists of a series of vectors with two components which can be easily evaluated from one set of expressions for each row of **Q** given above.

b-2) For Criss-Cross pattern:

Defining following factors

$$F_1 = 1-2\nu \qquad F_2 = -1+\nu \qquad F_3 = 1+\nu \qquad F_4 = 1+2\nu \qquad F_5 = -3+2\nu \qquad F_6 = -2+\nu$$
$$F_7 = -5+6\nu \quad F_8 = -4+7\nu \quad F_9 = -2+3\nu \quad F_{10} = -13+14\nu \quad F_{11} = -10+17\nu \quad F_{12} = 31-34\nu$$

$$G_1 = 2b^2F_2 - a^2F_1 \qquad G_2 = 2a^2F_2 - b^2F_1$$
$$G_3 = a^2b^2(5 + 4\nu(-3+2\nu)) \qquad G_4 = a^2b^2(-5 + 2(5-2\nu)\nu) \qquad G_5 = a^2b^2(1 + 2\nu - 4\nu^2)$$
$$G_6 = a^2b^2(11 + 4\nu(-7+6\nu)) \qquad G_7 = a^2b^2(23 + 4\nu(-11+6\nu)) \qquad G_8 = a^2b^2(81 + 68\nu(-3+2\nu))$$

$$H_1 = E^3(a^4 + 3a^2b^2 + b^4 - 3(a^2+b^2)^2\nu + 2(a^2+b^2)^2\nu^2)$$
$$H_2 = a^2b^2E^2F_3F_1(4b^4F_2\nu - a^4F_5F_1 + G_3) \qquad H_3 = a^2b^2E^2F_3F_1(4a^4F_2\nu - b^4F_5F_1 + G_3)$$
$$H_4 = a^4b^4E(F_3F_1)^2(2a^2\nu + b^2F_5)\alpha^2 \qquad H_5 = a^4b^4E(F_3F_1)^2(2b^2\nu + a^2F_5)\alpha^2$$
$$H_6 = E^3G_1(-a^4F_2F_1 + 3b^4F_2F_1 + G_4) \qquad H_7 = E^3G_2(-a^4F_2F_1 + 3b^4F_2F_1 + G_5)$$
$$H_8 = a^2b^2E^2F_3F_1(-4b^4F_6F_2 + G_6 - a^4F_{10}F_1)\alpha \qquad H_9 = a^2b^2E^2F_3F_1(4a^4F_2F_8 + b^4F_4F_1 + G_7)\alpha$$
$$H_{10} = a^6b^6(F_3F_1)^3\alpha^3$$
$$H_{11} = a^4b^4E(F_3F_1)^2(b^2F_7 + 2a^2F_8)\alpha^2 \qquad H_{12} = a^4b^4E(F_3F_1)^2(a^2F_7 + 2b^2F_8)\alpha^2$$
$$H_{13} = a^4b^4E(F_3F_1)^2(2a^2F_9 + b^2F_{10})\alpha^2 \qquad H_{14} = a^4b^4E(F_3F_1)^2(2b^2F_9 + a^2F_{10})\alpha^2$$
$$H_{15} = a^4b^4E(F_3F_1)^2(b^2F_7 + 2a^2F_9)\alpha^2 \qquad H_{16} = a^4b^4E(F_3F_1)^2(2b^2F_9 + a^2F_7)\alpha^2$$
$$H_{17} = E^2G_1(b^4F_2F_1 - G_5 - 3a^4F_2F_1) \qquad H_{18} = E^2G_2(b^4F_2F_1 - 3a^4F_2F_1 - G_4)$$

$$H_{19} = a^2b^2E^2F_3F_1(-4b^4F_2F_8 - G_7 - a^4F_4F_1)\alpha \qquad H_{20} = a^2b^2E^2F_3F_1(4a^4F_6F_2 + b^4F_{10}F_1 - G_6)\alpha$$
$$H_{21} = E^3(3a^4 + 7a^2b^2 + 3a^4 - 9(a^2 + b^2)^2\nu + 6(a^2 + b^2)^2\nu^2)$$
$$H_{22} = a^2b^2E^2F_3F_1(4b^4F_2F_{11} + a^4F_{12}F_1 + G_8)\alpha \qquad H_{23} = a^2b^2E^2F_3F_1(4a^4F_2F_{11} + b^4F_{12}F_1 + G_8)\alpha$$
$$H_{24} = E^2(2a^4 + 5a^2b^2 + 2b^4 - 6(a^2 + b^2)^2\nu + 4(a^2 + b^2)^2\nu^2)$$
$$H_{25} = F_3F_1(12b^2EF_2 - a^2F_1(6E + b^2F_3\alpha)) \qquad H_{26} = (-6b^2EF_1 + a^2(12EF_2 - b^2F_3F_1\alpha))$$

$$I_1 = -432H_1G_1 - 36H_2\alpha + 6H_4 + H_{10} \qquad I_2 = 864H_6 - 72H_8 + 12H_{11} - 2H_{10}$$
$$I_3 = -36H_{19} - 6H_{13} + H_{10} \qquad I_4 = 432H_{21}G_1 - 36H_{22} + 42H_{15} - 7H_{10}$$
$$I_5 = -432H_1G_2 - 36H_3\alpha + 6H_5 + H_{10} \qquad I_6 = 864H_7 - 72H_9 + 12H_{14} - 2H_{10}$$
$$I_7 = -36H_{20} - 6H_{12} + H_{10} \qquad I_8 = 432H_{21}G_2 - 36H_{23} + 42H_{16} - 7H_{10} \qquad \text{(B-8)}$$

Then the following expressions for elements of **Q** are obtained

$$Q_{11} = \frac{(I_1 + \mu_2(I_2 + I_1\mu_2) - 2\mu_1(432EH_{17} + I_3 - 2I_4\mu_2 + (432H_{17} + I_3)\mu_2^2) + \mu_1^2(I_1 + \mu_2(I_2 + I_1\mu_2)))}{(-96abH_{25}H_{26}\mu_1\mu_2)}$$

$$Q_{12} = Q_{21} = \frac{1}{(-8H_{25}H_{26}\mu_1\mu_2)}(E(36H_{24} - a^4b^4(F_3F_1)^2\alpha^2)(-1 + \mu_1^2)(-1 + \mu_2^2))$$

$$Q_{22} = \frac{(I_5 + \mu_2(I_6 + I_5\mu_2) - 2\mu_1(432EH_{18} + I_7 - 2I_8\mu_2 + (432H_{18} + I_7)\mu_2^2) + \mu_1^2(I_5 + \mu_2(I_6 + I_5\mu_2)))}{(-96abH_{25}H_{26}\mu_1\mu_2)}$$

(B-9)

REFERENCES

[1] Zienkiewicz, O.C. and Bettess, P., "Infinite elements in the study of fluid structure interaction problems", *Lecture Notes in Physics,* Vol. 58, Eds. J. Ehlers *et al.* Springer-Verlag, Berlin, 1976.

[2] Bettess, P. and Zienkiewicz, O.C., "Diffraction and refraction of surface waves using finite and infinite elements", *Int. J. Numer. Methods Eng.,* Vol. 11, pp. 1271–1290, 1977.

[3] Astley, R.J. and Eversman, W., " Finite element formulation for acoustical radiation", *J. Sound and Vibration.,* Vol. 88, pp. 47-64, 1983.

[4] Gerdes, K., "A summary of Infinite Element formulations for exterior Helmholtz problems" Comput. *Methods Appl. Mech. Engrg.* Vol. 164, pp.95-105, 1998.

[5] Astley, R.J., "Infinite elements for wave problems: a review of current formulations and assessment of accuracy", *Int. J. Numer. Methods Eng.,* Vol. 49, pp. 951–976, 2000.

[6] Zienkiewicz, O.C. and Taylor, R. L., "*The finite element method*", 5th edition, Butterworth-Heineman, 2000.

[7] Engquist, B. and Majda, A., "Absorbing boundary conditions for the numerical simulation of waves", *Math. Comp.* Vol. 31, pp. 629-651, 1977.

[8] Givoli, D. and Keller, J.B., "A finite element method for large domains", *Comput. Methods Appl. Mech. Engrg.* Vol.76, pp.41-66, 1989.

[9] Givoli, D., Patlashenkob, I. and Keller, J.B., "Discrete Dirichlet-to-Neumann maps for unbounded domains" *Comput. Methods Appl. Mech. Engrg.* Vol. 164, pp.173-185, 1998.

[10] Berenger, J.P., "A perfectly matched layer for the absorption of electromagnetic waves", *J. Comput. Phys.* Vol. 114, pp.185-200, 1994.

[11] Turkel , E. and Yefet, A., "Absorbing PML boundary layers for wave-like equations", *Appl. Numer. Math.,* Vol. 27, pp. 533-557, 1998.

[12] Shirron, J.J. and Babuška, I., "A comparison element of approximate boundary conditions and infinite methods for exterior Helmholtz problems" *Comput. Methods Appl. Mech. Engrg.* Vol.164, pp.121- 139, 1998.

[13] Tsynkov, S., "Numerical solution of problems on unbounded domains. A review". *Appl. Numer. Math.*, Vol. 27, pp. 465–532, 1998.

[14] Thatcher, T.W., "On the finite element method for unbounded regions", *SIAM J. Numer. Anal.,* Vol 15, No.5, pp. 466-477, 1978.

[15] Dasgupta G. "A finite element formulation for unbounded homogeneous continua". *ASME*. Vol. 49, pp. 136-140, 1982.

[16] Wolf, J.P. and Song, Ch., "*Finite-element Modelling of Unbounded Media*" (Wiley, 1996).

[17] Song, Ch. and Wolf, J.P., "The scaled boundary finite method-alias consistent infinitesimal fifnite element method- for elastodynamics". *Comput. Methods Appl. Mech. Engrg.* Vol.147, pp.239- 355, 1997.

[18] Wolf, J.P. "*The Scaled Boundary Finite Elemen Metodt*" (Wiley, 2003).

[19] Cherukuri, H. P. ''Dispersion analysis of numerical approximations to plane wave motions in an isotropic elastic solid." *Comput. Mech.,* Vol. 25, No.4, pp. 317–328, 2000.

[20] Ihlenburg, F. and Babuška, I., "Finite element solution of the Helmholtz equation with high wave number Part I: The h-version of the FEM" *Computers. Math. Applic.* Vol. 30, No. 9, pp.9-37, 1995.

[21] Ihlenburg, F and Babuška, I., "Dispersion analysis and error estimation of Galerkin finite element methods for the Helmholtz equation", *Int. J. Numer. Methods Eng.,* Vol. 38, pp. 3745-3774, 1995.

[22] Babuška, I., Ihlenburg, F., Strouboulis, T., Gangaraj, S.K. , "A posteriori error estimation for finite element solutions of Helmholtz' equations. Part I : the quality of local indicators and estimators.", *Int. J. Numer. Methods Eng.*, Vol. 40, No. 18, pp. 3443-3462, 1997.

[23] Babuška, I., Ihlenburg, F., Strouboulis, T., Gangaraj, S.K. , "A posteriori error estimation for finite element solutions of Helmholtz' equations. Part II : estimation of pollution error.", *Int. J. Numer. Methods Eng.*, Vol. 40, No. 21, pp. 3883-3900, 1997.

[24] Deraemaeker, A., Babuška, I., and Bouillard, P. ''Dispersion and pollution of the FEM solution for the Helmholtz equation in one, two and three dimensions.'' *Int. J. Numer. Methods Eng.,* Vol. 46, No.4, pp. 471–499, 1999.

[25] Harari, I., and Nogueira, C.L., "Reducing Dispersion of Linear Triangular Elements for the Helmholtz Equation" *J. Eng. Mech. (ASCE)*, Vol. 128, No. 3, pp. 351-358, 2002.

[26] Thompson, L.L. and Pinsky, P.M., "A Galerkin Least-Squares Finite Element Method for the Two-Dimensional Helmholtz Equation" .", *Int. J. Numer. Methods Eng.*, Vol. 38, pp. 371-397, 1995.

[27] Wolf, J.P. "*Soil-Structure-Interaction Analysis in Time Domain*" Prentice-Hall, 1988.

List of figures